



The microRNA/TET3/REST axis is required for olfactory globose basal cell proliferation and male behavior

Dong Yang , Xiangbo Wu, Yanfen Zhou, Weina Wang & Zhenshan Wang* 

Abstract

In the main olfactory epithelium (MOE), new olfactory sensory neurons (OSNs) are persistently generated to replace lost neurons throughout an organism's lifespan. This process predominantly depends on the proliferation of globose basal cells (GBCs), the actively dividing stem cells in the MOE. Here, by using CRISPR/Cas9 and RNAi coupled with adeno-associated virus (AAV) nose delivery approaches, we demonstrated that knockdown of miR-200b/a in the MOE resulted in supernumerary Mash1-marked GBCs and decreased numbers of differentiated OSNs, accompanied by abrogation of male behaviors. We further showed that in the MOE, miR-200b/a targets the ten-eleven translocation methylcytosine dioxygenase TET3, which cooperates with RE1-silencing transcription factor (REST) to exert their functions. Deficiencies including proliferation, differentiation, and behaviors illustrated in miR-200b/a knockdown mice were rescued by suppressing either TET3 or REST. Our work describes a mechanism of coordination of GBC proliferation and differentiation in the MOE and olfactory male behaviors through miR-200/TET3/REST signaling.

Keywords CRISPR-Cas9; differentiation and proliferation; globose basal cell; main olfactory epithelium; olfactory male behaviors

Subject Categories Chromatin, Transcription, & Genomics; Neuroscience; RNA Biology

DOI 10.15252/embr.201949431 | Received 7 October 2019 | Revised 14 June 2020 | Accepted 18 June 2020 | Published online 17 July 2020

EMBO Reports (2020) 21: e49431

Introduction

The main olfactory epithelium (MOE) in mammals detects external olfactory stimuli. Moreover, the MOE plays a crucial role in male–male aggressive behavior, male–female sexual behavior, and other activities (Dulac & Torello, 2003).

As a pseudostratified neuroepithelium, the MOE consists of several cell types, including horizontal basal cells (HBCs), globose basal cells (GBCs), immature olfactory sensory neurons (iOSNs), mature olfactory sensory neurons (mOSNs), and sustentacular

(SUS) cells (Beites *et al.*, 2005). OSNs are generated by two types of stem cells: the frequently dividing GBCs and the dormant HBCs (Leung *et al.*, 2007). In the intact MOE, GBCs are the major pool of proliferative progenitors, while HBCs act as a reserve stem cell pool and remain dormant unless activated by MOE injury (Caggiano *et al.*, 1994; Fletcher *et al.*, 2017; Gadye *et al.*, 2017). Neurogenesis is sustained throughout the lifespan in the MOE (Caggiano *et al.*, 1994; Schwob *et al.*, 1994). Given that the MOE is in direct contact with the varying external environment, its neurogenesis is modified by numerous epigenetic factors, including microRNAs (miRNAs) (Sokpor *et al.*, 2018). Accordingly, the MOE is an appropriate peripheral tissue to examine how adult neurogenesis is sculpted by these epigenetic factors.

As epigenetic factors, miRNAs regulate gene expression by binding to the 3' untranslated region (UTR) sequences of their target mRNAs (Bartel, 2009). Numerous miRNAs act at the post-transcriptional level to regulate the expression of genes involved in proliferation, differentiation, survival, and apoptosis in various cell types (Rajman & Schratt, 2017). In addition, certain miRNAs have been implicated in various *in vivo* behaviors; for example, miR-182/96/183 and miR-9 are involved in learning and memory (Sim *et al.*, 2016; Woldemichael *et al.*, 2016), the miR379-410 cluster is involved in hypersocial behavior (Lackinger *et al.*, 2019), and miR-128 is related to fear-extinction memory and motor behavior (Lin *et al.*, 2011; Tan *et al.*, 2013).

The miR-200 family, as one of the best-studied miRNA families, has been shown to modulate numerous biological processes, such as pluripotent stem cell generation (Wang *et al.*, 2013), female fertility (Hasuwa *et al.*, 2013), pancreatic beta cell survival (Belgardt *et al.*, 2015), and puberty initiation (Messina *et al.*, 2016). The miR-200 family is highly enriched in the MOE, and studies with Dicer knockout mice and antisense morpholino oligonucleotides complementary to its hairpin sequences in one-cell zebrafish showed that this family may play pivotal roles in olfactory neurogenesis of the embryonic MOE (Choi *et al.*, 2008; Garaffo *et al.*, 2015). However, the biological significance of the miR-200 family and the underlying molecular mechanisms in the post-natal mammals remain elusive.

Here, by using intranasal delivery of adeno-associated virus (AAV)-CRISPR/Cas9 to knockdown genes exclusively in the MOE, we provide evidence that miR-200b/a is critical for GBC

proliferation and differentiation and olfactory-mediated behaviors in adult mice. Mechanistically, we show that in the MOE, miR-200b/a regulates TET3, a ten-eleven translocation methylcytosine dioxygenase that interacts with RE1-silencing transcription factor (REST, also known as neuron-restrictive silencing factor, NRSF). Furthermore, the deficiencies induced by miR-200b/a knockdown (KD) were rescued by suppressing either TET3 or REST in the MOE. Therefore, our work indicates that miR-200b/a, TET3, and REST function together in the MOE to contribute to the proliferation and differentiation of GBCs and olfactory-mediated male behaviors in adult mice.

Results

miR-200b and miR-200a in the MOE are indispensable for olfactory-mediated male behaviors

In most OSNs, the odorant detection is dependent primarily on the cAMP signal transduction pathway, which consists of odorant receptors (ORs), Golf, type III adenylyl cyclase (AC3), and the cyclic nucleotide-gated ion channel (CNG channel) (Brunet *et al*, 1996; Belluscio *et al*, 1998; Wong *et al*, 2000). AC3 is an essential component of this cAMP olfactory pathway, and AC3 knockout mouse (AC3^{-/-}) showed typical dysosmia (Wong *et al*, 2000). In addition, it has been revealed that the stabilization of OR expression and maturation of OSNs are regulated by AC3 through epigenetic mechanisms (Lyons *et al*, 2013). To explore the correlation between olfactory function and epigenetic factors especially miRNA expression, we sequenced small RNAs from MOE tissues dissected from adult AC3^{-/-} and AC3^{+/+} mice. Small RNA profiling showed that 18 were significantly upregulated and 23 were dramatically downregulated in AC3^{-/-} mice compared to AC3^{+/+} mice (Appendix Fig S1A and B and Dataset EV1). miR-200b and miR-200a displayed the highest abundance (Appendix Fig S1B and C) and were much higher than the other differentially expressed miRNAs in the MOE (Appendix Fig S1B and C). Accordingly, we focused our efforts on the potential functions of miR-200b and miR-200a in the subsequent studies.

Quantitative real-time PCR (qPCR) analyses of the MOEs of AC3^{-/-} and AC3^{+/+} mice demonstrated that the miR-200b and miR-200a levels were dramatically lower in the AC3^{-/-} mice than in the AC3^{+/+} mice (Appendix Fig S1D). However, in the brain, testis, and liver, miR-200b and miR-200a were not significantly downregulated in the AC3^{-/-} mice compared with the AC3^{+/+} mice (Appendix Fig S1E–G). These data suggest that miR-200b and miR-200a are positively regulated by AC3 in the MOEs.

For analysis of their physiologically significant roles, miR-200b and miR-200a were simultaneously knocked down in the MOE of adult mice by a combination of CRISPR-Cas9 and intranasal delivery of AAV. As the miR-200b/a cluster is transcribed from a common promoter and located adjacent to mouse chromosome 4, single guide RNAs (sgRNAs) targeting the left arm (F') of miR-200b and the right arm (R') of miR-200a were designed (Appendix Fig S2A). The most efficient sgRNAs (target 2 for the F' arm and target 4 for the R' arm, Appendix Fig S2B and C) were identified and utilized in subsequent studies. We employed a dual-vector system in which SpCas9 (AAV-SpCas9) and sgRNA expression cassettes (AAV-Guide

RNA) were packaged into two AAV2/9 vectors (Appendix Fig S2D; detailed in the Materials and Methods section). Mice aged between 4 and 6 weeks were perfused with viral vectors (Cas9 AAV coupled with miR-200b/a sgRNAs or normal control [NC] sgRNA AAV) at a one-to-one ratio via the intranasal route (Fig 1A).

To determine the optimum time course required for AAV-Cas9 to infect the mouse MOE for improved infectivity, we analyzed the Cas9 protein expression in the mouse MOE tissues after 2, 3, 6, and 8 weeks of AAV intranasal perfusion. The cells positive for Cas9 should be the cells infected by AAV. The results of immunofluorescence (IF) staining showed that the number of Cas9⁺ cells in the MOE perfused by AAV increased with the extension of infection time (Appendix Fig S3A–C). At the 8th week after perfusion, the number of Cas9⁺ cells in the MOE of the NC mice was 50.54 ± 2.759 cells/mm and that of the miR-200b/a KD mice was 49.44 ± 3.021 cells/mm, indicating that the AAV infection efficiency of the two groups of mice was indistinguishable (Appendix Fig S3C). Other studies have shown that at least 6 weeks were required for the best knockdown effect following CRISPR-Cas9-mediated AAV injection *in vivo* (Long *et al*, 2016; Yang *et al*, 2016; Yu *et al*, 2017). Therefore, we used the mice perfused with AAV in the nasal cavity for 8 weeks to carry out the subsequent experiments, unless mentioned otherwise.

We observed significantly reduced miR-200b and miR-200a expression in the MOE of the miR-200b/a KD mice at 8 weeks after perfusion (Fig 1B). However, in the hypothalamus (a downstream signaling organ of the MOE), the levels of miR-200b and miR-200a were indistinguishable between the miR-200b/a KD mice and their NC controls (Appendix Fig S3D). In addition, qPCR showed that the expression of *Till10*, the host gene of miR-200b/a, in the MOE was indistinguishable between the miR-200b/a KD mice and the NC controls (Fig 1C). Furthermore, next-generation sequencing (NGS) analysis of the predicted possible off-target sites (information in Dataset EV2) showed no off-target editing in the MOE of the miR-200b/a KD mice (Appendix Fig S3E and F). Taken together, our results strongly confirmed that miR-200b/a were knocked down in the MOE 8 weeks after intranasal viral perfusion.

Behavioral performance was observed in a cohort of animals 8 weeks after intranasal viral perfusion. The locomotor activity of the miR-200b/a KD mice was indistinguishable from that of the NC animals (Fig 1D). Then, an odorant habituation test (Trinh & Storm, 2003) was performed to examine whether olfactory detection was abrogated in the MOE of the miR-200b/a KD mice. Compared with their NC controls, the miR-200b/a KD mice exhibited severely compromised detection of the odorants tested (Fig 1E).

Both male–male aggressive and male–female mating behaviors are MOE dependent (Pfeiffer & Johnston, 1994). We explored the male–male aggressive behavior of the miR-200b/a KD mice using a resident/intruder assay. Although the NC controls invariably attacked the male intruder, in the miR-200b/a KD mice, the attack frequency and duration toward the intruder males were dramatically reduced (Fig 1F and G). Male–female mating behavior was assayed by introducing a sexually receptive, unfamiliar, wild-type female into the tested male home cage. Although the NC controls displayed mounting as well as intromission behaviors toward the females, the mounting frequency and duration toward the females of the miR-200b/a KD mice were significantly reduced (Fig 1H and I).

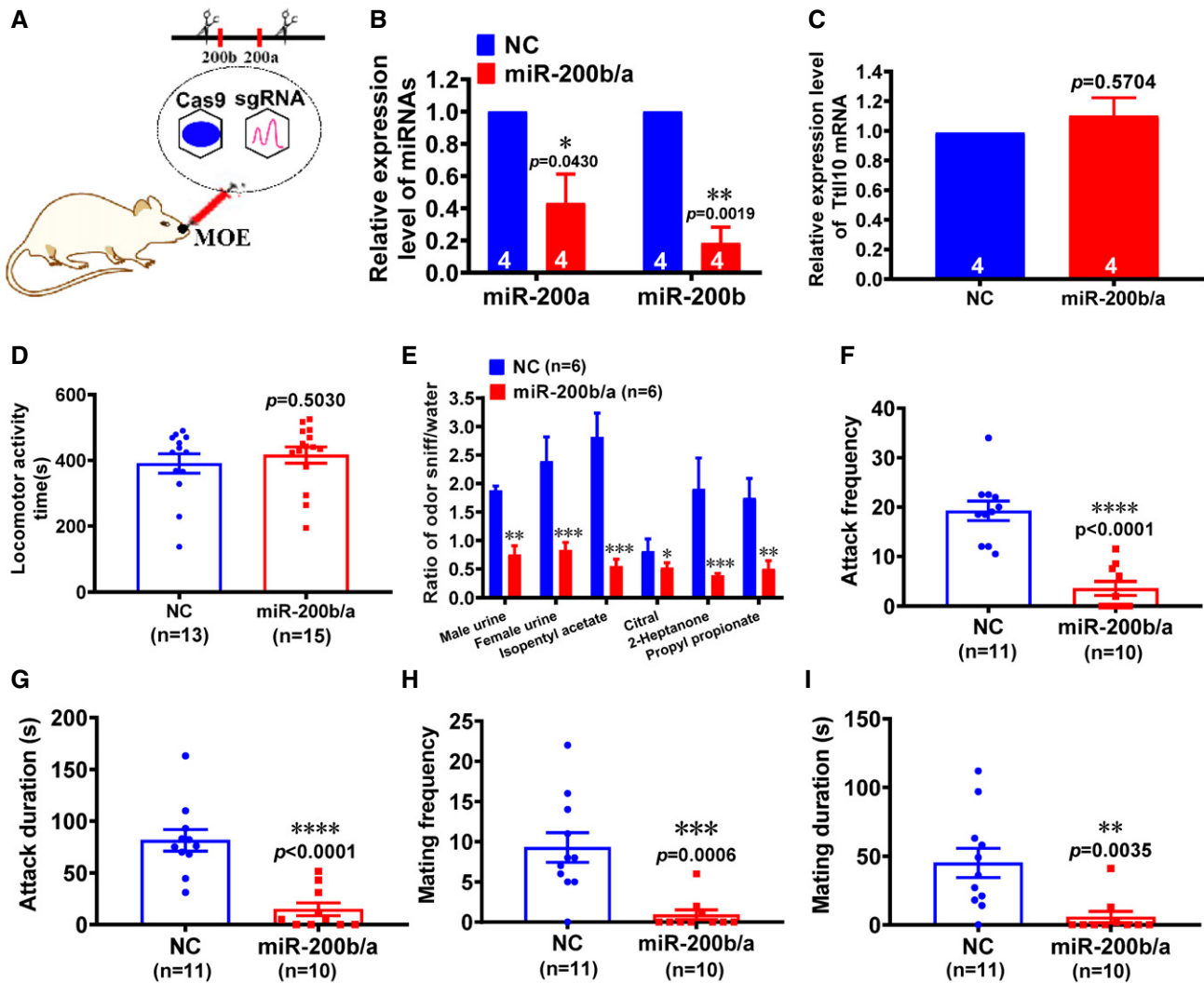


Figure 1. miR-200b/a are critical for olfactory-mediated male behaviors.

- A** Schematic illustration of intranasal delivery of AAV into the MOE.
- B** The expression of mature miR-200b and miR-200a in the MOE of the NC and miR-200b/a KD mice, as revealed by qPCR analysis ($n = 4$ mice each group; data represent the mean \pm SEM; * $P < 0.05$, ** $P < 0.01$; Student's *t*-test).
- C** The expression of Ttl10 (the host gene of miR-200b/a) mRNA in the MOE of the NC and miR-200b/a KD mice, as revealed by qPCR analysis ($n = 4$ mice each group; data represent the mean \pm SEM; $P = 0.3540$; Student's *t*-test).
- D** The locomotor activity of the miR-200b/a KD mice was similar to that of the NC mice (NC: $n = 13$ mice, miR-200b/a knockdown: $n = 15$ mice; data represent the mean \pm SEM; $P = 0.5030$; Student's *t*-test).
- E** The odorant habituation results shown as the ratio of odor sniffs/water of the miR-200b/a KD mice were significantly reduced compared to those of the NC mice. These odorants included male urine (1:50), female urine (1:50), isopentyl acetate (50 μ M), citral (50 μ M), 2-heptanone (50 μ M), and propyl propionate (50 μ M) ($n = 6$ mice each group; data represent the mean \pm SEM; * $P < 0.05$, ** $P < 0.01$, *** $P < 0.001$; Student's *t*-test).
- F, G** The resident/intruder experiment showed that the attack frequency (F) and duration (G) of the miR-200b/a KD mice were impaired compared to those of the NC mice (NC: $n = 11$ mice, miR-200b/a KD: $n = 10$ mice; data represent the mean \pm SEM; **** $P < 0.0001$; Student's *t*-test).
- H, I** The analysis of male–female mating behaviors showed that the mating frequency (H) and duration (I) of the miR-200b/a KD mice were significantly reduced compared to those of the NC mice (NC: $n = 11$ mice, miR-200b/a KD: $n = 10$ mice; data represent the mean \pm SEM; ** $P < 0.01$, **** $P < 0.001$; Student's *t*-test).

Taken together, these results indicate that miR-200b/a in the MOE are essential for olfactory-guided male behaviors.

miR-200b/a are crucial for the Mash1-marked GBC proliferation

To explore the underlying mechanisms of the impaired olfactory-mediated male behaviors, we dissected the MOE tissues of the

miR-200b/a KD mice and their NC controls at 8 weeks after intranasal viral perfusion for RNA transcriptome analysis. Overall, we detected significant changes in the expression of 4427 mRNAs (Appendix Fig S4A and Dataset EV3) between the miR-200b/a KD mice and their NC controls. By integrating our transcriptome sequencing results with Colquitt's dataset (Colquitt *et al.*, 2013), we found that in miR-200b/a KD mice, 627 of 654 upregulated genes

were HBC/GBC specific and 13 were mOSN specific; of the 795 downregulated genes, 46 were HBC/GBC specific and 160 were mOSN specific (Fig 2A and Dataset EV4). These findings indicate that most of the genes involved in GBC development are upregulated, while most of the genes involved in differentiated neurons are downregulated.

In the MOE, the GBC population accounted for 97.6% of all active proliferating progenitors (Huard & Schwob, 1995). Ki67 is a proliferation marker expressed during all active phases of the proliferating cell cycle. To investigate the proliferation of GBCs, the MOE sections were immunolabeled with antibodies against Ki67. The IF staining results showed that the numbers of Ki67⁺ cells were significantly increased in the miR-200b/a KD mice compared with the NC controls (Fig 2B and C). The result suggests that the proliferation of GBCs is promoted in mice with miR-200b/a downregulation in the MOE.

The cell cycle exit of progenitor cells involves a switch from proliferation to differentiation. For generation of appropriate numbers and subtypes of neurons at the right time and place, developmental control of the cell cycle exit must be finely regulated. We examined the cell cycle exit index of GBCs by incorporating EdU labeling and Ki67 antibody assays 24 h after EdU injection. Under these conditions, cells that exited the cell cycle should be EdU⁺ and Ki67⁻, whereas cells that are still cycling should be positive for both markers. MOE staining showed that the numbers of costained Ki67⁺ and EdU⁺ cells were significantly higher in the miR-200b/a KD mice than in their NC controls (Fig 2D and E). The proportion of GBCs that exited the cell cycle was dramatically reduced in the miR-200b/a KD mice compared with their NC controls (Fig 2D and F), indicating that the cell cycle exit of GBCs is suppressed in the MOE of the mice with miR-200b/a knockdown.

The division modes of neural progenitors have been correlated with their cell cycle dynamics (Dehay & Kennedy, 2007). To obtain the S phase length of the GBC progenitors, we intraperitoneally injected BrdU (100 mg/kg body weight) into the NC mice and the miR-200b/a KD mice, and EdU (50 mg/kg body weight) was injected intraperitoneally into these mice 3 h later. The mice were sacrificed 45 min later to dissect the MOE tissues for staining with the BrdU antibody and EdU detection kit. For the observation of the total length of the GBC cell cycle, we injected BrdU (100 mg/kg weight) intraperitoneally into the NC mice and the miR-200b/a KD mice and then injected EdU (50 mg/kg weight) 20 h later. After injection of EdU for 45 min, the MOE tissues were dissected for IF with the BrdU antibody and EdU detection kit. According to the Brandt *et al* (2012) formula and the proportion of BrdU⁺/BrdU⁺EdU⁻ cells, the S phase length of the GBCs in the MOE of the miR-200b/a KD mice increased significantly compared with that of the NC mice (Fig 2G and H). However, there was no difference in the total cell cycle length of the GBCs between the MOE of the NC mice and the miR-200b/a KD mice (NC vs. miR-200b/a KD: 22.55 ± 0.074 h vs. 22.53 ± 0.5461 h, Fig 2I). Recent studies have also revealed that the transition of neuronal progenitors from proliferation to differentiation (neurogenic) is specifically associated with the duration of S phase (Brandt *et al*, 2012; Soufi & Dalton, 2016). Therefore, consistent with the RNA transcriptome analysis results, our cell cycle observation results further demonstrated that reduction of miR-200b/a in the MOE promoted proliferation and suppressed the cell cycle

exit of the GBC populations along with an increased S phase duration.

To confirm the proliferative observations in cellular compositions in more detail, we investigated markers representing various developmental cell types of the MOE (Fig 3A) with qPCR, Western blot analysis, and IF staining. Cytokeratin 14 (CK14) and Trp63 are two markers exclusively expressed in HBCs. The qPCR and IF staining results showed that the expression of CK14 and Trp63 was indistinguishable between the miR-200b/a KD mice and their NC controls (Fig 3B–D), implying that the number of HBCs was not altered in the MOE of the mice with miR-200b/a knockdown. SUS cells are generated from HBCs (Fletcher *et al*, 2017) and are specifically labeled by antibodies against Sox2 at the apical MOE (Lin *et al*, 2017). IF staining with a Sox2 antibody showed that the Sox2⁺ cells from the apical MOE were comparable between the miR-200b/a KD mice and their NC controls (Fig 3C and D), indicating that miR-200b/a is dispensable for SUS cells. GBCs exclusively express basal Sox2 and Mash1 (Ascl1) markers in developmental sequence. qPCR, Western blot, and IF analyses for basal Sox2 showed that the expression of this marker was indistinguishable between the miR-200b/a KD mice and the NC controls (Fig 3B–E), suggesting that the number of basal Sox2⁺ GBCs was comparable between these animals. However, qPCR, Western blot, and IF analyses indicated that there were significantly more Mash1⁺ GBCs in the MOE of the miR-200b/a KD mice than in the MOE of their NC controls (Fig 3B–E). Strikingly, some Mash1⁺ cells even expanded into the OSN layer (Fig 3C), which is normally immunonegative for Mash1.

To further confirm that the increase in Mash1-positive cells in the MOE is due to the knockdown of miR-200b/a, we injected EdU into the mice perfused with AAV for 8 weeks and sacrificed the mice 2 h later. The MOE tissues were costained with antibodies for Mash1 or Sox2 and EdU. The results of IF costaining showed that there was no difference in the number of EdU⁺/Sox2⁺ cells between the MOE of the NC controls and the miR-200b/a KD mice (Fig 3F and G). Compared with the NC controls, the number of EdU⁺/Mash1⁺ cells in the MOE of the miR-200b/a KD mice increased significantly (Fig 3H and I), indicating that the increase in GBCs was involved the Mash1-positive cells. We also costained the Cas9 protein with various cell type markers in the MOE. The results showed that the Cas9⁺/Mash1⁺ cells constituted $87.39 \pm 1.266\%$ and that of Cas9⁺/GAP43⁺ cells constituted $6.26 \pm 0.595\%$ of the total number of Cas9⁺ cells (Fig EV1A and B). There was no colocalization with OMP and CK14 (Fig EV1A and B). These results further indicated that the increase in Mash1-positive cells in the MOE is due to the knockdown of miR-200b/a. The Cas9 staining data indicated that the Cas9 integrated into the genome mainly occurred in the basal GBCs. It is well established that the integration of Cas9 into the target locus is influenced by many factors, such as sequences in and around the target, sgRNA sequences, and cell types (Miyaoaka *et al*, 2016; Cai *et al*, 2019). In addition, it has been revealed that the chromatin accessibility is a major determinant of Cas9 binding (Wu *et al*, 2014; Horlbeck *et al*, 2016; Isaac *et al*, 2016; Yarrington *et al*, 2018; Liu *et al*, 2019, 2020). In nondividing cells, the chromatin dynamics may be more relative static. More importantly, the intranasal delivery AAV method utilized in this study executes a narrow time window to Cas9 and/or sgRNA access. Nevertheless, our Cas9 staining results

are in accordance with the fact that incorporated Cas9 in the host DNA in mammalian brain is primarily limited to the dividing cells (Mikuni et al, 2016; Nishiyama et al, 2017; Nami et al, 2018).

Taken together, these data indicate that appropriate miR-200b/a expression in the MOE is indispensable for the maintenance of proper levels of Mash1⁺ GBCs.

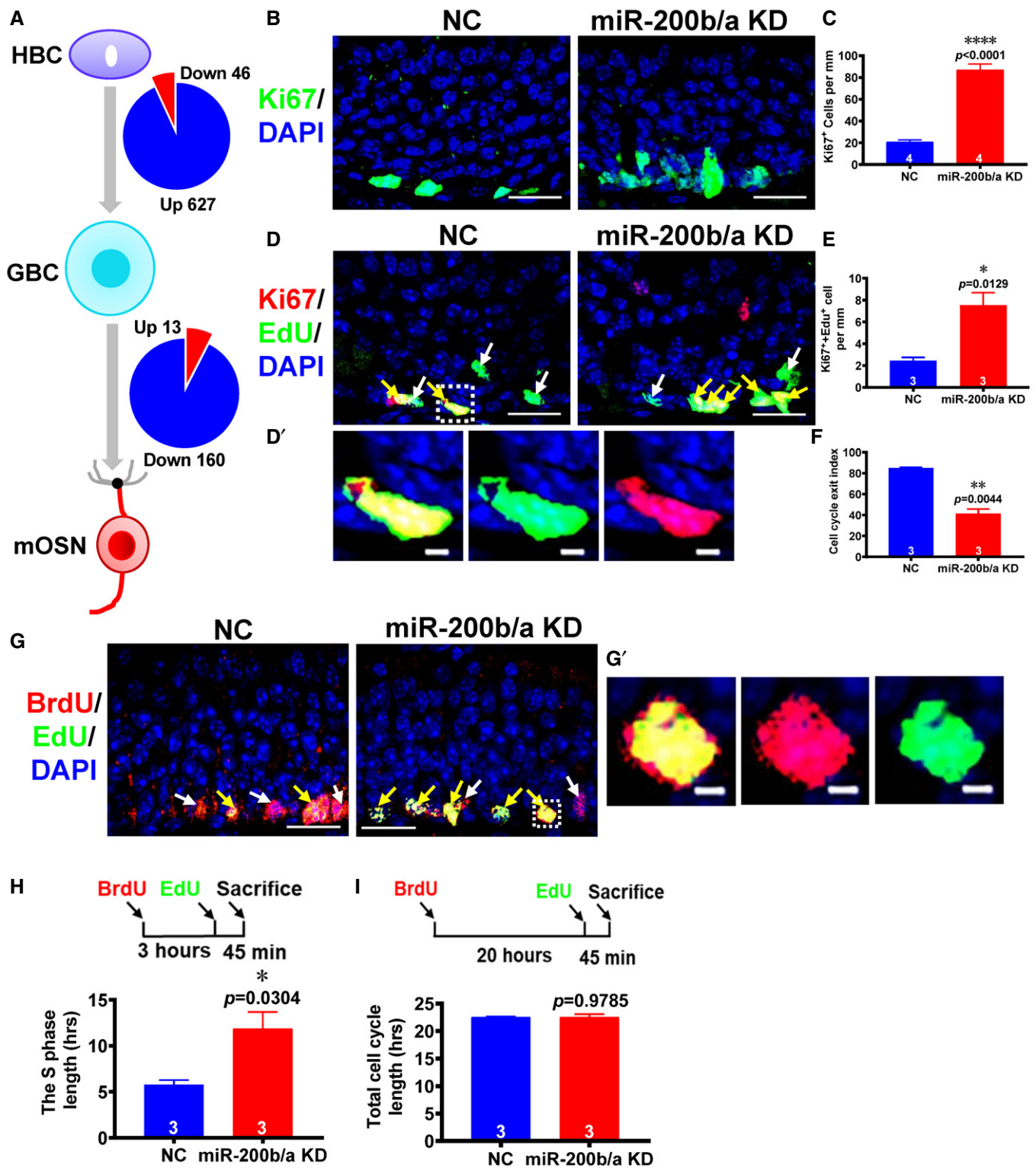


Figure 2.

Figure 2. miR-200b/a are crucial for the proliferation and the cell cycle of GBCs.

- A The number of genes differentially and exclusively expressed in different olfactory cells of the MOE in the NC and miR-200b/a KD mice identified by RNA sequencing.
- B Representative IF staining with Ki67 antibody in the MOE of the NC and miR-200b/a KD mice. Scale bars, 20 μ m.
- C Quantification of the numbers of Ki67⁺ cells in the MOE of the NC and miR-200b/a KD mice ($n = 4$ mice each group; data represent the mean \pm SEM; ** $P < 0.01$, **** $P < 0.0001$; Student's t -test).
- D Representative IF costaining with both EdU and Ki67 antibody in the MOE of the NC and miR-200b/a KD mice. The white arrows indicate the EdU⁺ cells, and the yellow arrows indicate the cells positive for both EdU and Ki67. (D') is shown at higher magnification of the boxed region, as three-channel merged images (left image) and the separated channel (middle and right images). (D): Scale bars, 20 μ m; (D'): Scale bars, 2 μ m.
- E Quantification of the numbers of costained Ki67⁺ and EdU⁺ cells in the MOE of the NC and miR-200b/a KD mice ($n = 3$ mice each group; data represent the mean \pm SEM; * $P < 0.05$; Student's t -test).
- F The proportion of GBCs that exited the cell cycle was significantly reduced in the miR-200b/a KD mice compared with their NC controls (the cell cycle exit index was calculated using the following formula: $[\text{EdU}^+ \text{Ki67}^- \text{ cells} / \text{total EdU}^+ \text{ cells}] \times 100$; $n = 3$ mice each group; data represent the mean \pm SEM; ** $P < 0.01$; Student's t -test).
- G Representative IF costaining with both EdU and BrdU antibody in the MOE of the NC and miR-200b/a KD mice. The white arrows indicate the BrdU⁺ cells, and the yellow arrows indicate the cells positive for both BrdU and EdU. (G') is shown at higher magnification of the boxed region, as three-channel merged images (left image) and the separated channel (middle and right images). (G): Scale bars, 20 μ m; (G'): Scale bars, 2 μ m.
- H The S phase length of the GBCs in the MOE of the NC and miR-200b/a KD mice (the S phase length was calculated using the following formula: $3 \text{ h} \times \text{BrdU}^+ / \text{BrdU}^+ \text{EdU}^-$; $n = 3$ mice each group; data represent the mean \pm SEM; * $P < 0.05$; Student's t -test).
- I Total cell cycle length of the GBCs in the MOE of the NC and miR-200b/a KD mice (total cell cycle length was calculated using the following formula: $20 \text{ h} + (\text{Ts} \times \text{EdU}^+ \text{BrdU}^- / \text{EdU}^+)$; $n = 3$ mice each group; $P = 0.9785$; data represent the mean \pm SEM; Student's t -test).

The differentiated neurons are reduced in mice with miR-200b/a knockdown in the MOE

Differentiated neurons are specifically labeled by the marker Tuj1. IF staining showed that the number of Tuj1⁺ neurons was dramatically decreased in the miR-200b/a KD mice compared with their NC controls (Fig 4A and B), suggesting that the miR-200b/a KD mice had fewer differentiated neurons than the control mice. Consistent with the Tuj1 data, qPCR and IF analyses showed that the numbers of Ngn1⁺, GAP43⁺, and OMP⁺ OSNs were significantly reduced in the miR-200b/a KD mice compared with their NC controls (Fig 4A–C).

In the MOE, the OSNs are exclusively differentiated from GBCs. To confirm that the reduction of OSNs in the miR-200b/a KD mice was due to the decreased differentiation of GBCs in the MOE, we injected BrdU intraperitoneally in the miR-200b/a KD mice and the NC controls at 8 weeks after intranasal AAV-Cas9 perfusion. The time between BrdU injection and perfusion can be used to map the fate of recently generated OSNs, as identified by their incorporation of BrdU. It has been revealed that a newborn OSN requires 24 h to differentiate into an iOSN, and until 3 days after BrdU injection, a corresponding fraction of BrdU⁺ cells is GAP43 positive (Liberia *et al*, 2019). Therefore, we perfused the mice at 3 days after BrdU injection for analysis of GBC differentiation. The costaining results showed that the BrdU⁺/GAP43⁺ cells accounted for $18.30 \pm 0.7709\%$ of the total GAP43⁺ cells in the NC mice (Fig 4D and E). The results were consistent with previous studies (Coleman *et al*, 2017; Liberia *et al*, 2019). However, in the MOE of the miR-200b/a KD mice, the number of BrdU⁺/GAP43⁺ cells was only $1.007 \pm 0.1217\%$ of the GAP43⁺ cells (Fig 4D and E). This finding suggested that the differentiation of GBCs into OSNs is weakened after miR-200b/a knockdown, which results in decreased numbers of OSNs.

Olfactory sensory neurons reduction is often accompanied by a high level of apoptosis (Mahalik, 1996; Wang *et al*, 2012). Olfactory receptor genes (olfrs) expression is required for the survival and maturation of OSNs (Iwema & Schwob, 2003). Our RNA transcriptome sequencing results showed that the expression of many olfrs decreased in the MOE of the miR-200b/a KD mice. Accordingly, we

speculate that high levels of apoptosis may be one of the reasons for the decrease of the number of OSNs in the miR-200b/a KD mice. As a typical marker of apoptosis, caspase-3 (Cas3) expression represents the level of apoptosis. We detected the cell apoptosis in the mice with AAV nasal perfusion for 8 weeks. The Cas3 IF results showed that in the mice with AAV nasal perfusion for 8 weeks, the number of Cas3-positive cells in the miR-200b/a KD mice increased significantly compared with that in the NC mice (Fig 4F and G).

Although increases in Cas3 cells were observed in the MOE of the miR-200b/a KD mice after 8 weeks AAV nasal perfusion, the total number of GBCs, OSNs, and Cas3⁺ cells was comparable between the NC controls and the miR-200b/a KD mice (Appendix Fig S4B). Hematoxylin–eosin (HE) staining further indicated that the gross and microscopic anatomy of the MOE was comparable between the miR-200b/a KD mice and their NC controls (Appendix Fig S4C).

Taken together, these data indicate that appropriate expression of miR-200b/a in the MOE is crucial for GBC differentiation into OSNs. Furthermore, high levels of apoptosis can also reduce the number of olfactory neurons in the MOE of the miR-200b/a KD mice.

TET3 is directly regulated by miR-200b/a in the MOE

A striking feature of our MOE RNA expression profile was that 1111 of 1181 olfrs were downregulated in the miR-200b/a KD mice (Fig 5A and Dataset EV5) compared with their NC controls, consistent with the finding in TET3-TG mice that identified 1071 downregulated olfrs of 1082 olfrs (Colquitt *et al*, 2013). Given that olfr mRNAs have a short 3' UTR and few predicted miRNA-binding sites (Shum *et al*, 2015), these olfrs are probably not directly regulated by miR-200b/a in the MOE.

Given the RNA sequencing data in TET3-TG mice (Colquitt *et al*, 2013), our data, and the finding that the cell cycle progression of cerebral cortex neural progenitors depends on miRNAs through TET3 targeting (Lv *et al*, 2014), we speculated that the miR-200b/a functions may be mediated by targeting TET3 to maintain a dynamic equilibrium between proliferation and differentiation in GBCs. Indeed, prediction by TargetScan algorithms showed that the 3' UTR

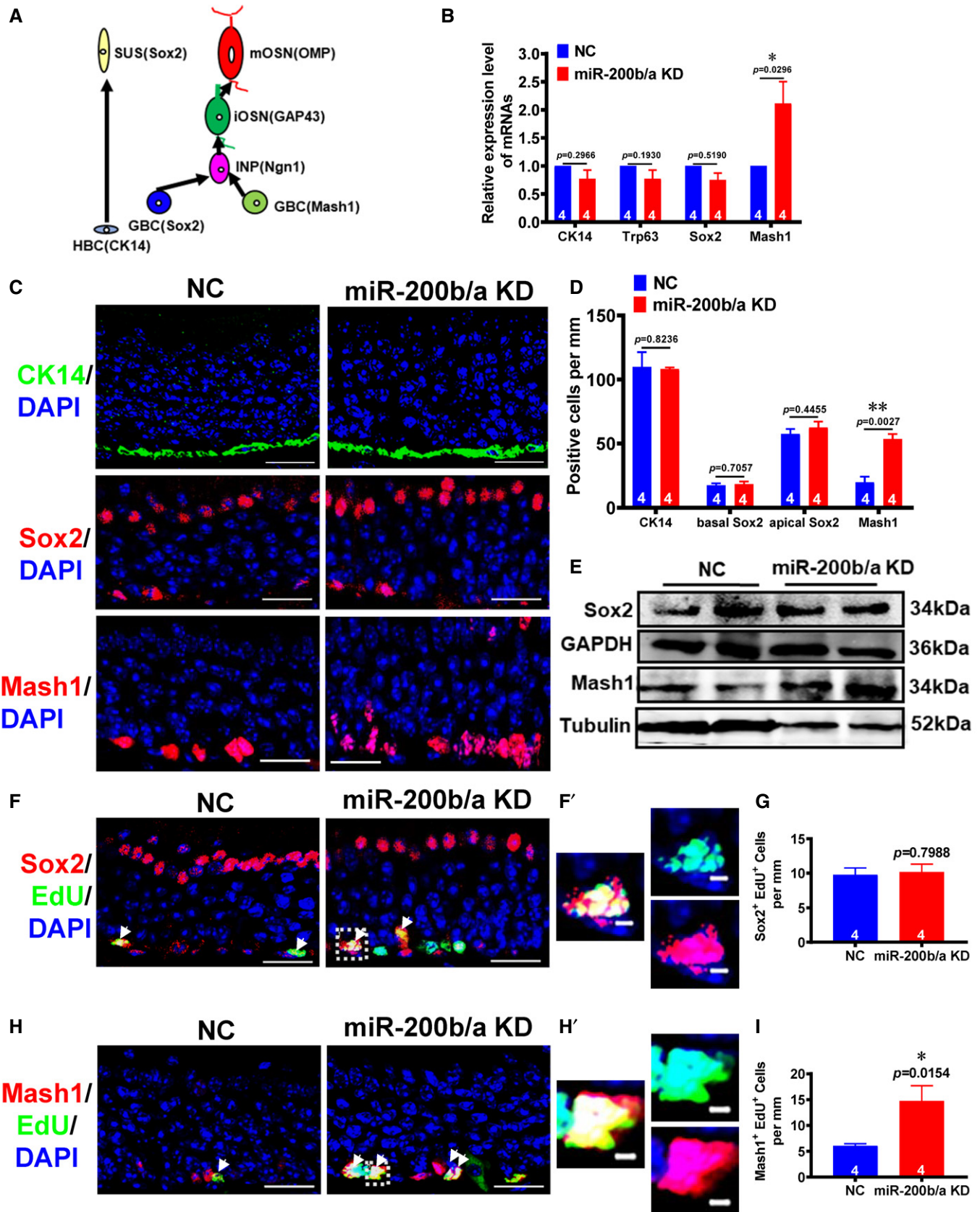


Figure 3.

Figure 3. miR-200b/a are crucial for the proliferation of the Mash1-marked GBCs.

- A Schematic illustration of developmentally expressed olfactory cell types: horizontal basal cell (HBC), globose basal cell (GBC), intermediate nerve progenitor (INP), and immature olfactory sensory neuron (iOSN), mature olfactory sensory neuron (mOSN), and sustentacular cell (Sus).
- B The mRNA levels of CK14, Trp63, Sox2, and Mash1 in the MOE of the NC and miR-200b/a KD mice, as revealed by qPCR analysis ($n = 4$ mice each group; data represent the mean \pm SEM; CK14: $P = 0.2135$, Trp63: $P = 0.1930$, Sox2: $P = 0.5190$, $*P < 0.05$; Student's *t*-test).
- C Representative IF staining for CK14, Sox2, and Mash1 in the MOE of the NC and miR-200b/a KD mice. Scale bars, 20 μ m.
- D Quantification of the number of CK14⁺, basal Sox2⁺, apical Sox2⁺, and Mash1⁺ cells in the MOE of the NC and miR-200b/a KD mice ($n = 4$ mice each group; data represent the mean \pm SEM; CK14: $P = 0.8998$, basal Sox2: $P = 0.7056$, apical Sox2: $P = 0.4455$, $**P < 0.01$; Student's *t*-test).
- E Western blot analysis of the Sox2 and Mash1 protein levels in the MOE of the NC and miR-200b/a KD mice ($n = 2$ mice each group). GAPDH and Tubulin served as loading controls. The molecular weight of each band is indicated at the right.
- F Representative IF costaining with Sox2 antibody and EdU in the MOE of the NC and miR-200b/a KD mice. The white arrows indicate the cells positive for both Sox2 and EdU. (F') is shown at higher magnification of the boxed region, as three-channel merged images (left image) and the separated channel (right images). (F): Scale bars, 20 μ m; (F'): Scale bars, 2 μ m.
- G Quantification of the number of Sox2⁺ EdU⁺ cells in the MOE of the NC and miR-200b/a KD mice ($n = 4$ mice each group; data represent the mean \pm SEM; $P = 0.7988$; Student's *t*-test).
- H Representative IF costaining with Mash1 antibody and EdU in the MOE of the NC and miR-200b/a KD mice. The white arrows indicate the cells positive for both Mash1 and EdU. (H') is shown at higher magnification of the boxed region, as three-channel merged images (left image) and the separated channel (right images). (H): Scale bars, 20 μ m; (H'): Scale bars, 2 μ m.
- I Quantification of the number of Mash1⁺ EdU⁺ cells in the MOE of the NC and miR-200b/a KD mice ($n = 4$ mice each group; data represent the mean \pm SEM; $*P < 0.05$; Student's *t*-test).

of TET3 harbors a miR-200a binding site, which is highly conserved from *Xenopus* to humans (Fig 5B).

The partial mouse TET3 3' UTR containing the predicted miR-200a target site was then cloned into a dual-luciferase reporter, which showed that ectopic miR-200a expression suppressed luciferase activity. In contrast, a mutation in the putative miR-200a seed region in the TET3 3' UTR abrogated the suppression by miR-200a (Fig 5C), suggesting that miR-200a represses TET3 expression through the predicted target site in the TET3 3' UTR. Meanwhile, in 3T3-L1 cells with miR-200a inhibitor or mimic transfection, qPCR and Western blot analyses confirmed that endogenous TET3 is indeed regulated by miR-200a (Fig 5D–F).

In vivo analysis after miR-200a mimic and no-target mimic injection into the MOE demonstrated that miR-200a regulates TET3 expression (Fig 5G). However, the miR-200b-binding site was not identified within the 3' UTR of TET3 by the TargetScan algorithms. The targeted sequences of miR-200a and miR-200b only differ by one nucleotide, and for each miR-200, ~30% of the targets are recognized without seed matches (Hoefert *et al*, 2018). We also confirmed that the expression of TET3 in the MOE is regulated by miR-200b (Fig 5H). Furthermore, qPCR, Western blot, and IF analyses of the MOE tissues from the miR-200b/a knockdown and NC control animals demonstrated that TET3 was significantly elevated in the miR-200b/a KD mice compared to the NC controls (Fig 5I–K and Appendix Fig S5A). Considering that TET3 can oxidize 5-methylcytosine (5mC) to 5-hydroxymethylcytosine (5hmC) and is highly enriched in the MOE (Fig 5I and J), to further confirm the increase of TET3, we performed IF staining to investigate the levels of 5mC and 5hmC in the MOE and found that miR-200b/a knockdown dramatically reduced the levels of 5mC (Fig 5L and M) but significantly increased the levels of 5hmC (Fig 5N and O). These results indicate that TET3 is regulated by miR-200b/a in the MOE.

Given that TET1 and TET2 are also expressed in the MOE (Colquitt *et al*, 2013), we examined their expression in the MOE of these mice. qPCR and Western blot analyses showed that the expression of TET1 and TET2 in the MOE was indistinguishable between the miR-200b/a KD mice and their NC controls (Appendix Fig S5A and B), excluding the possibility that the expression of TET1 and TET2 is also regulated by miR-200b/a in the MOE.

Although Foxg1 was proposed to be a potential target of the miR-200 family in zebrafish (Choi *et al*, 2008; Garaffo *et al*, 2015), we did not find any binding sites within its 3' UTR with TargetScan algorithms. Furthermore, our qPCR and IF results showed that the Foxg1 level in the MOE was comparable between the miR-200b/a KD mice and their NC controls (Appendix Fig S5C–E), indicating that miR-200b/a did not directly target Foxg1 to exert their functions in the mouse MOE.

Taken together, our data indicate that TET3 is regulated by miR-200b/a in the MOE.

The behavioral and GBC differentiation deficiencies induced by miR-200b/a knockdown are partially reversed by TET3 suppression

Given that TET3 is required for adult neurogenesis (Montalban-Loro *et al*, 2019) and regulated by miR-15b (Lv *et al*, 2014) and that Mash1⁺ GBCs are proliferative progenitors that generate OSNs, we hypothesized that the Mash1⁺ cell increase and GBC neuronal differentiation deficiency induced by miR-200b/a knockdown in the MOE can be attributed to the abnormal increase in TET3 expression. To this end, IF costaining for TET3 and Mash1 was performed to explore whether the increase in the number of TET3⁺ cells induced by miR-200b/a knockdown in the MOE mainly included Mash1⁺ cells. Indeed, the number of TET3⁺/Mash1⁺ cells, which were located at the base of the MOE, was much higher in the miR-200b/a KD mice than in the NC mice (Fig 6A and B). To further confirm this point, we simultaneously knocked down miR-200b/a and TET3 in the MOE by injections of Cas9 + miR-200b/a sgRNAs + TET3 sgRNA AAV into the noses of 4- to 6-week-old mice (Appendix Fig S6A), with animals perfused with either Cas9 + NC sgRNA or Cas9 + miR-200b/a sgRNAs as the controls (Appendix Fig S6A). The knockdown efficiency was ascertained 8 weeks after AAV perfusion. qPCR and IF staining showed that TET3 was restored to the NC level in the miR-200b/a + TET3 double knockdown (miR-200b/a + TET3 DKD) mice (Appendix Fig S6B–D). Given that the TET3 gRNA sequences used here were identical to those previously employed (Ito *et al*, 2010), DNA sequence analysis for the identification of off-target editing was not performed again in this study.

Male–male aggressive behavioral tests showed that the duration of the attack on intruders performed by the miR-200b/a + TET3 DKD mice was significantly improved compared with that of the miR-200b/a KD mice, although the duration did not completely return to the levels observed in the NC mice (Fig 6C and D). In contrast, the mating performance indicated by the frequency and duration of mating to females was comparable between the miR-200b/a KD mice and the miR-200b/a + TET3 DKD mice and differed

from the normal male–female mating performance demonstrated by the NC males (Fig 6E and F). These results indicated that the male–male aggressive deficiency induced by miR-200b/a knockdown was partially restored by suppressing TET3 expression in the MOE, whereas the male sexual behavioral deficiencies were not ameliorated.

Immunofluorescence staining showed that the level of Mash1⁺, Cas3⁺, and Ki67⁺ cells in the MOE of the miR-200b/a + TET3 DKD

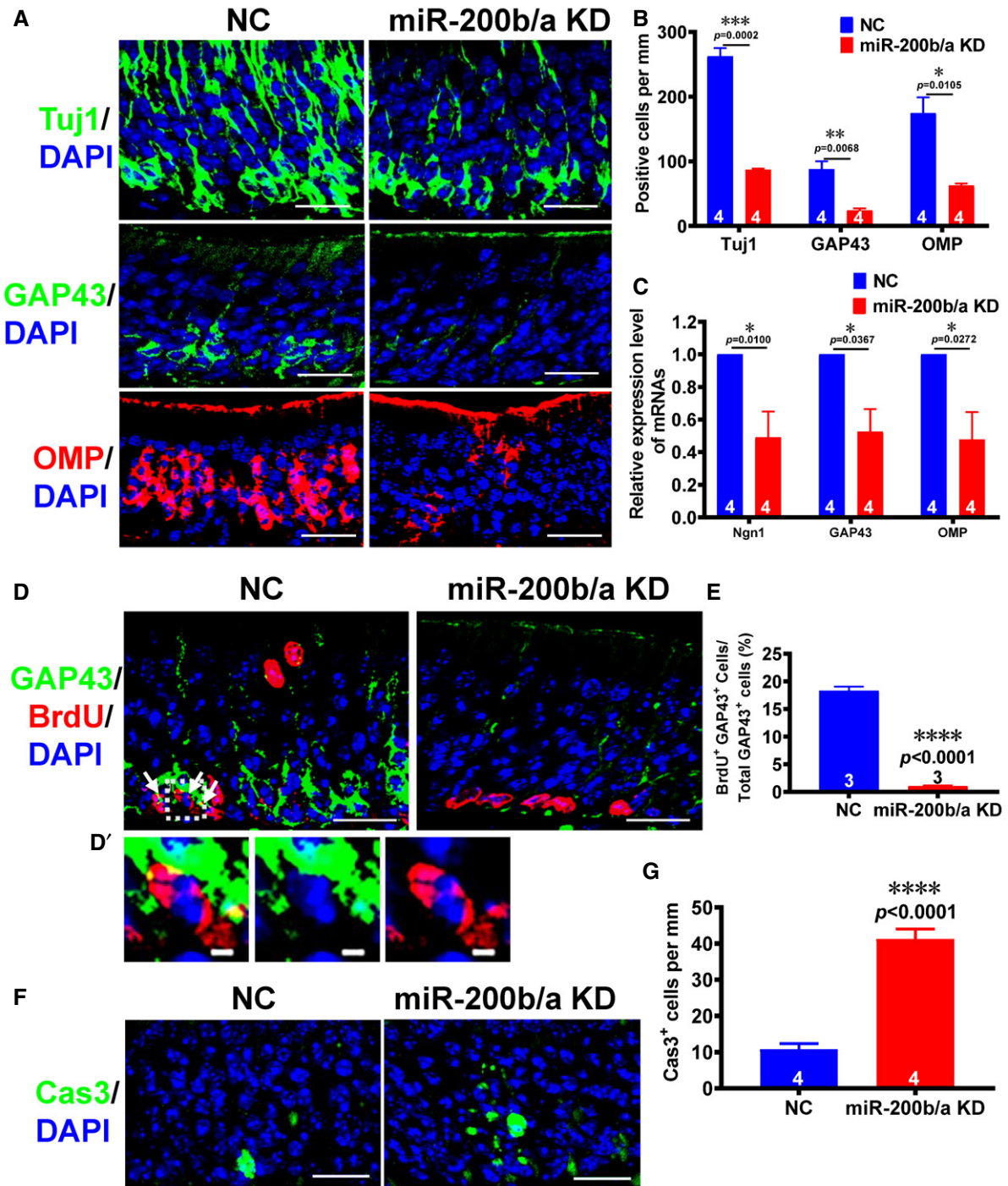


Figure 4.

Figure 4. miR-200b/a are crucial for the differentiation of OSNs.

- A Representative IF staining for Tuj1, GAP43, and OMP in the MOE of the NC and miR-200b/a KD mice. Scale bars, 20 μ m.
- B Quantification of the number of Tuj1⁺, GAP43⁺, and OMP⁺ cells in the MOE of the NC and miR-200b/a KD mice ($n = 4$ mice each group; data represent the mean \pm SEM; * $P < 0.05$, ** $P < 0.01$, *** $P < 0.001$; Student's t -test).
- C The mRNA levels of Ngn1, GAP43, and OMP in the MOE of the NC and miR-200b/a KD mice, as revealed by qPCR analysis ($n = 4$ mice each group; data represent the mean \pm SEM; * $P < 0.05$; Student's t -test).
- D Representative IF costaining with GAP43 and BrdU antibodies in the MOE of the NC and miR-200b/a KD mice injected with BrdU at 3 days. The white arrows indicate the cells positive for both GAP43 and BrdU. (D') is shown at higher magnification of the boxed region, as three-channel merged images (left image) and the separated channel (middle and right images). (D): Scale bars, 20 μ m; (D'): Scale bars, 2 μ m.
- E Quantification of the ratio of the number of BrdU⁺ GAP43⁺ cells and the number of total GAP43⁺ cells in the MOE of the NC and miR-200b/a KD mice injected with BrdU at 3 days ($n = 3$ mice each group; data represent the mean \pm SEM; **** $P < 0.0001$; Student's t -test).
- F Representative IF staining with Cas3 antibody in the MOE of the NC and miR-200b/a KD mice. Scale bars, 20 μ m.
- G Quantification of the number of Cas3⁺ cells in the MOE of the NC and miR-200b/a KD mice ($n = 4$ mice each group; data represent the mean \pm SEM; *** $P < 0.001$; Student's t -test).

mice was reduced to the level in the NC mice (Fig 6G, H, J and K). Similarly, the number of Tuj1-labeled OSNs was significantly increased by double knockdown, although it did not reach that of the NC control (Fig 6G and I). Collectively, these results indicate that the effects of the GBC proliferation abnormalities and reductions in differentiated OSNs induced by miR-200b/a knockdown in the MOE could be countered by TET3 suppression. Thus, we illustrate that not only the male–male aggressive behavior deficiency but also the impaired proliferation and differentiation of GBCs induced by miR-200b/a knockdown could be, at least partially, reverted to the normal phenotype by suppressing TET3 in the MOE, implying that miR-200b/a-mediated TET3 is essential for these elements.

TET3 cooperation with REST is critical for GBC proliferation and differentiation

Previous studies have shown that TET3 forms a protein–protein complex with REST to cooperatively function in the mouse retina (Perera *et al*, 2015) and hypothalamus (Cramer *et al*, 2019). To explore the relationship between TET3 and REST in the MOE, we first detected the expression of REST in the miR-200b/a KD and miR-200b/a + TET3 DKD mouse MOE. qPCR showed that the expression of REST was significantly higher in the miR-200b/a KD mouse MOE than in the NC mouse MOE (Fig 7A). In the miR-200b/a + TET3 DKD mice, the expression of REST mRNA was not significantly altered compared with that in the miR-200b/a KD mice (Fig 7A). However, Western blot and IF analyses demonstrated that the expression of REST in the MOE of the miR-200b/a KD mice was significantly higher than that in the MOE of the NC mice, while in the miR-200b/a + TET3 DKD mouse MOE, the REST expression level was restored to the NC level (Fig 7B–D). These findings suggest that in the MOE, TET3 may regulate the expression of REST at the protein level but not at the transcriptional level. REST and Mash1 costaining was then performed on MOE tissues, revealing that the number of REST⁺/Mash1⁺ cells was significantly increased in the MOE of the miR-200b/a KD mice compared to that in the NC mice (Fig 7E and F). Since both available commercial antibodies of TET3 and REST are from the same host (rabbit polyclonal), the costaining of these two antibodies is extremely challenge. Given the costaining of REST and Mash1, and TET3 and Mash1 mentioned above, we speculated that REST and TET3 are coexpressed in the increased Mash1⁺ GBCs induced by miR-200b/a knockdown in the MOE.

To verify whether REST interacts with TET3 in the MOE, we performed a reciprocal coimmunoprecipitation (co-IP) analysis with lysates of the MOE using antibodies against the TET3 and REST proteins. Immunoblot analysis performed using a REST antibody in the MOE lysates immunoprecipitated with the anti-TET3 antibody showed REST immunoactivity in the MOE lysates immunoprecipitated with the anti-TET3 antibody (Fig 7G). Similarly, immunoblot analysis performed using a TET3 antibody in the MOE lysates immunoprecipitated with the anti-REST antibody showed TET3 immunoactivity in the MOE lysates immunoprecipitated with the anti-REST antibody (Fig 7H). These results suggest that endogenous TET3 and REST are interacted in the MOE.

Considering that REST and TET3 work cooperatively as a complex in the MOE and that REST is critical for neurogenesis, the abnormal REST upregulation induced by miR-200b/a knockdown through targeting TET3 is expected to be the cause of the deficiencies in GBC proliferation and differentiation. Accordingly, the impaired phenotypes induced by miR-200b/a knockdown in the MOE should be ameliorated by suppressing REST expression. Due to the existence of multiple splice variants, REST knockout by conventional targeting excision in the genome may not be effective for all isoforms (Mampay & Sheridan, 2019). Accordingly, we employed an RNAi approach to knockdown REST in the mouse MOE.

The optimal knockdown effect of CRISPR/Cas9 induced by *in vivo* AAV injection requires 6–8 weeks (Appendix Fig S3B and C) (Long *et al*, 2016; Yang *et al*, 2016; Yu *et al*, 2017). AAV-mediated RNAi can achieve the optimal knockdown effect *in vivo* at 3–4 weeks (Chadderton *et al*, 2009; Foust *et al*, 2013). To obtain mice with knockdown of both miR-200b/a and REST in the MOE, we first knocked down miR-200b/a in the mice by the Cas9 and sgRNA AAV approach with a 5-week infection period and then knocked down REST in these mice by intranasal injection of shRNA AAV with a 3-week infection period. We also used animals treated with Cas9 + nontargeting NC oligo AAV injection and miR-200b/a KD mice as negative controls (Fig EV2A). Then, the MOE tissues from these mice were dissected for qPCR, Western blot, and IF analyses. All results showed that the expression of REST in the miR-200b/a + REST double knockdown (miR-200b/a + REST DKD) mice was comparable to that of the NC controls and significantly lower than that of the miR-200b/a KD mice (Fig EV2B–E).

Subsequently, the male aggression and mating performance in these mice were observed to determine whether the male

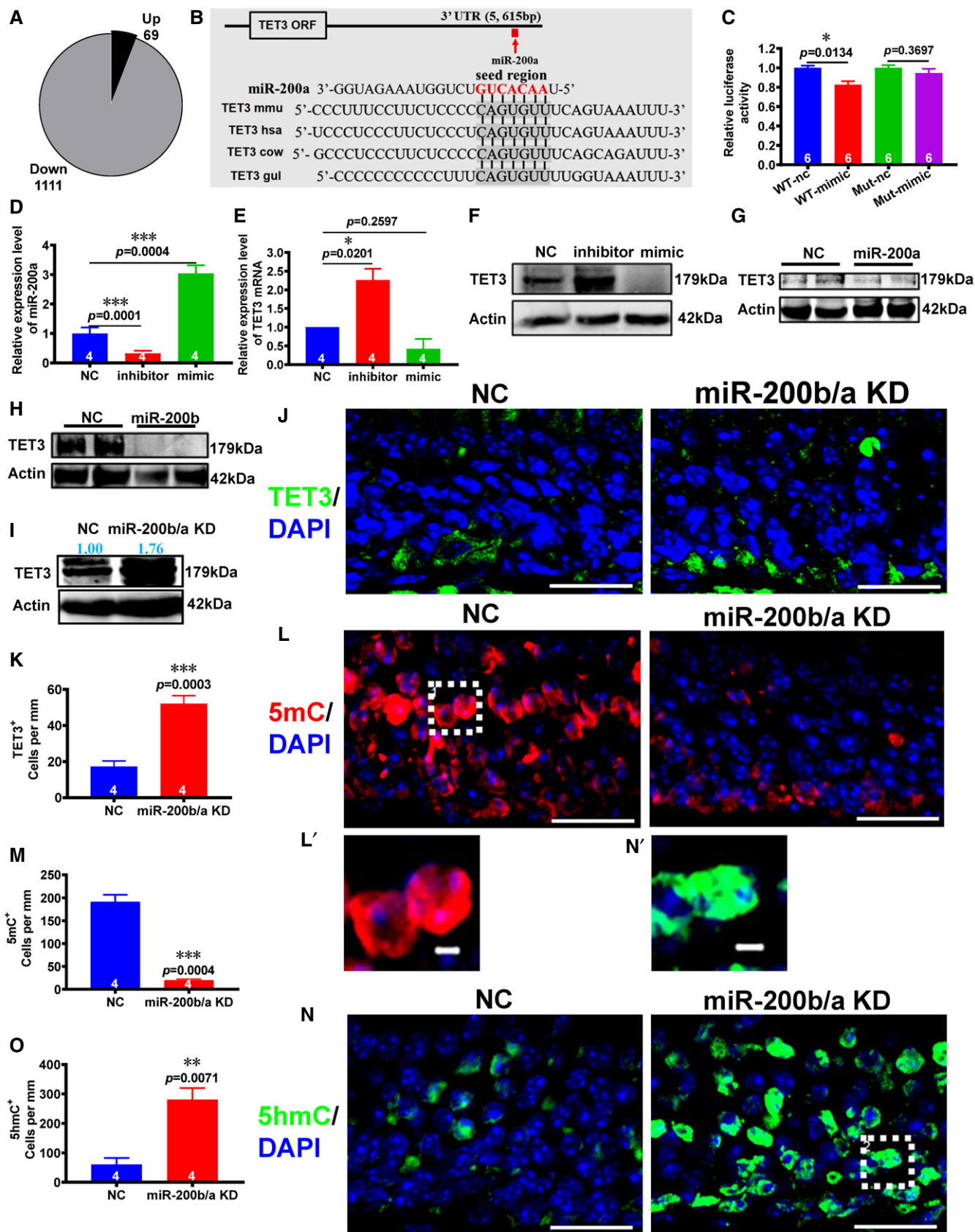


Figure 5.

Figure 5. TET3 is directly regulated by miR-200b/a in the 3T3-L1 cells and the MOE.

- A The number of differentially expressed olfirs from RNA sequencing in the MOE of the NC and miR-200b/a KD mice.
- B Schematic illustration of the predicted binding between miR-200a and the TET3 3' UTR.
- C TET3 3' UTR-dependent expression of a luciferase reporter gene was suppressed by miR-200a overexpression. Luciferase reporter gene under the control of the wild-type (WT) or mutant (Mut) TET3 3' UTR was transfected along with the negative control (nc) RNA or miR-200a mimic duplexes into HeLa cells ($n = 6$ from six independent experiments; data represent the mean \pm SEM; Mut-nc vs. Mut-mimic: $P = 0.3697$, $*P < 0.05$; Student's t -test).
- D, E The expression of mature miR-200a (D) and TET3 (E) mRNA in the 3T3-L1 cells treated with miR-200a inhibitor, miR-200a mimic, or control, as revealed by qPCR analysis ($n = 4$ from four independent experiments; data represent the mean \pm SEM; D: $F = 66.37$, E: $F = 16.39$, NC vs. mimic: $P = 0.2597$, $*P < 0.05$, $***P < 0.001$; one-way ANOVA and Bonferroni pairwise comparisons).
- F Western blot analysis of the TET3 protein level in the 3T3-L1 cells treated with miR-200a inhibitor, miR-200a mimic, or control ($n = 3$ from three independent experiments). Actin served as a loading control. The molecular weight of each band is indicated at the right.
- G, H Western blot analysis of the TET3 protein level in the MOE of the mice intranasally injected with miR-200a (G) or miR-200b (H) or NC mimic ($n = 3$ mice each group). Actin served as a loading control. The molecular weight of each band is indicated at the right.
- I Western blot analysis of the TET3 protein level in the MOE of the NC and miR-200b/a KD mice ($n = 3$ mice each group). Actin served as a loading control. The molecular weight of each band is indicated at the right. The blue number shows the ratio of the average intensity of TET3/Actin.
- J Representative IF staining of TET3 in the MOE of the NC and miR-200b/a KD mice. Scale bars: 20 μ m.
- K Quantification of the number of TET3⁺ cells in the MOE of the NC and miR-200b/a KD mice ($n = 4$ mice each group; data represent the mean \pm SEM; $***P < 0.001$; Student's t -test).
- L Representative IF staining of 5mC in the MOE of the NC and miR-200b/a knockdown mice. (L') is shown at higher magnification of the boxed region. (L): Scale bars, 20 μ m; (L'): Scale bars, 2 μ m.
- M Quantification of the number of 5mC⁺ cells in the MOE of the NC and miR-200b/a KD mice ($n = 4$ mice each group; data represent the mean \pm SEM; $***P < 0.001$; Student's t -test).
- N Representative IF staining of 5hmC in the MOE of the NC and miR-200b/a knockdown mice. (N') is shown at higher magnification of the boxed region. (N): Scale bars, 20 μ m; (N'): Scale bars, 2 μ m.
- O Quantification of the number of 5hmC⁺ cells in the MOE of the NC and miR-200b/a KD mice ($n = 4$ mice each group; data represent the mean \pm SEM; $**P < 0.01$; Student's t -test).

behavioral deficiency induced by miR-200b/a knockdown in the MOE was recaptured by REST knockdown. The male aggression and mating behaviors of the miR-200b/a + REST DKD mice were similar to those of the animals treated with Cas9 + nontargeting NC oligo AAV injection (Fig 8A–D). Therefore, these results indicate that appropriate REST expression mediated by miR-200b/a in the MOE is essential for male mating and aggressive behaviors.

Immunofluorescence staining showed that the numbers of Mash1⁺, Tuj1⁺, Cas3⁺, and Ki67⁺ cells in the MOE of miR-200b/a + REST DKD mice were comparable to those of the animals treated with Cas9 + nontargeting NC oligo AAV injection (Fig 8E–I). These results indicate that the deficits in GBC differentiation, apoptosis, and proliferation induced by miR-200b/a knockdown in the MOE are ameliorated by suppressing REST expression.

Discussion

In this study, we provided convincing evidence for the role of miR-200b/a in olfactory-mediated behaviors and GBC proliferation and differentiation and identified TET3 as a miR-200b/a target in the MOE. Furthermore, we demonstrated that TET3 cooperates with REST to exert its functions in the MOE. Thus, we firmly demonstrated that the miR-200b/a/TET3/REST regulatory cascade is indispensable for olfactory-mediated behaviors and GBC proliferation and differentiation in the mouse MOE.

Dicer is a key enzyme that processes pre-miRNA into individual mature miRNAs. Choi *et al* (2008) reported not only embryonic lethality but also MOE developmental arrest and degeneration in mice with Dicer specifically eliminated in olfactory progenitor cells, whereas the elimination of Dicer in mOSNs did not result in abnormal phenotypes. Paradoxically, the researchers also revealed that the miR-200 family is primarily restricted to the OSN layers and is

absent in the basal cell layers of the mouse MOE (Choi *et al*, 2008). Because all miR-200 family members were silenced by antisense morpholino oligonucleotides in embryos, zebrafish olfactory progenitors showed abnormal apoptosis and terminal differentiation (Choi *et al*, 2008; Garaffo *et al*, 2015). Based on these results, the researchers concluded that the miR-200 family is essential for terminal differentiation and the maintenance of olfactory neuronal progenitors in zebrafish embryos, although the detailed underlying mechanisms are not yet disclosed (Choi *et al*, 2008; Garaffo *et al*, 2015). The activity of a single miR-200 member is spatially and temporally specific (Brabletz & Brabletz, 2010); in some cases, a particular miR-200 miRNA promotes the differentiation of pluripotent or dedifferentiated stem cells, whereas in other cases, it inhibits this process (Gill *et al*, 2012).

Although analogous cell types have been identified in zebrafish, the stratification of the MOE is inconspicuous, as the different cell types do not segregate into three layers (Hansen & Zeiske, 1998). Accordingly, the results from zebrafish cannot be equated with those from mice. In addition, the above studies have not elucidated the biological role of the miR-200 family in the adult MOE. Regardless, in the present study, our data showed that maintaining an appropriate level of miR-200b/a expression in the MOE is essential for olfactory-mediated male behaviors in adult male mice. We further showed that adult mice with miR-200b/a knockdown in the MOE displayed fewer OSNs and more GBCs, as well as increased proliferation and suppressed cell cycle exit of GBCs. Consistent with our findings, disruptions in the proliferation, cell cycle exit, and neuronal differentiation of neural progenitor cells have been demonstrated in mice with deletion of the miR-200 family in the ventral hypothalamus of mouse embryos (Peng *et al*, 2012). Nevertheless, our study coupled with others (Choi *et al*, 2008; Garaffo *et al*, 2015; Fan *et al*, 2017) significantly extends the current understanding of the biological roles and the underlying mechanism of miRNAs in the mouse MOE.

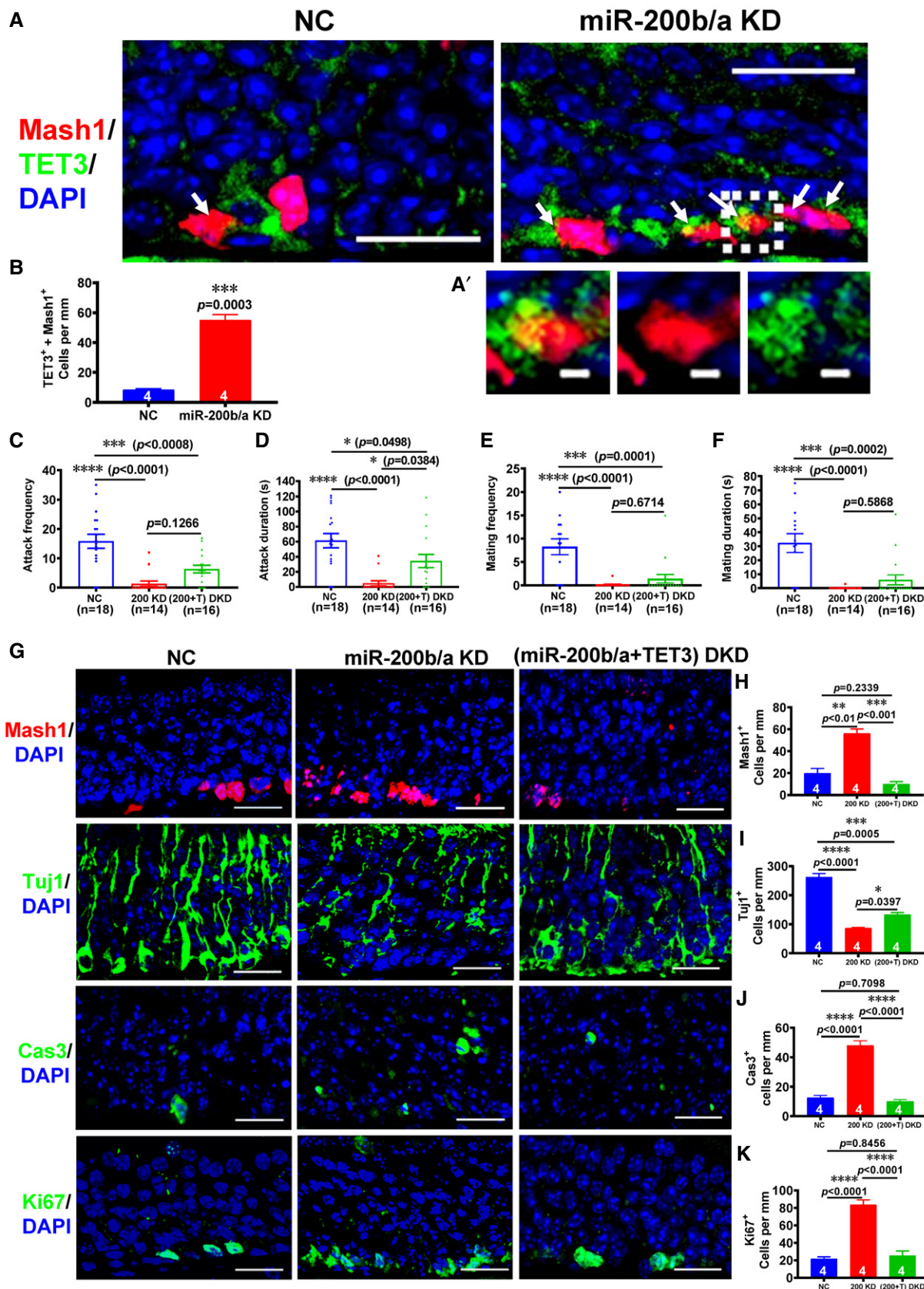


Figure 6.

Figure 6. The behavioral and GBC differentiation deficiencies induced by miR-200b/a knockdown are partially reversed by TET3 suppression.

- A Representative IF staining for costaining with TET3 and Mash1 antibodies in the MOE of the NC and miR-200b/a KD mice. The white arrows indicate the cells positive for both TET3 and Mash1. (A') is shown at higher magnification of the boxed region, as three-channel merged images (left image) and the separated channel (middle and right images). (A): Scale bars, 20 μ m; (A'): Scale bars, 2 μ m.
- B Quantification of the number of costained TET3⁺ and Mash1⁺ cells in the MOE of the NC and miR-200b/a KD mice ($n = 4$ mice each group; data represent the mean \pm SEM; *** $P < 0.001$; Student's t -test).
- C, D The resident/intruder experiment showed that the attack frequency (C) and duration (D) of the miR-200b/a + TET3 DKD mice were significantly improved compared with those of the miR-200b/a KD controls (200 KD: miR-200b/a KD; [200 + T] DKD: [miR-200b/a + TET3] DKD; [NC: $n = 18$ mice, miR-200b/a KD: $n = 14$ mice, miR-200b/a + TET3 DKD: $n = 16$ mice; data represent the mean \pm SEM; C: $F = 17.84$, D: $F = 12.06$, * $P < 0.05$, *** $P < 0.001$, **** $P < 0.0001$; one-way ANOVA and Bonferroni pairwise comparisons]).
- E, F The analysis of male–female mating behaviors showed that the frequency (E) and duration (F) of mating to females of the miR-200b/a + TET3 DKD mice were significantly reduced compared with those of their NC controls and were not dramatically different compared with those of the miR-200b/a KD mice (NC: $n = 18$ mice, miR-200b/a KD: $n = 14$ mice, miR-200b/a + TET3 DKD: $n = 16$ mice; data represent the mean \pm SEM; E: $F = 15.62$, F: $F = 15.56$, *** $P < 0.001$, **** $P < 0.0001$; one-way ANOVA and Bonferroni pairwise comparisons).
- G Representative IF staining for Mash1, Tuj1, Cas3, and Ki67 in the MOE of the NC, miR-200b/a KD, and miR-200b/a + TET3 DKD mice. Scale bars: 20 μ m.
- H–K Quantification of the numbers of Mash1⁺ (H), Tuj1⁺ (I), Cas3⁺ (J), and Ki67⁺ (K) cells in the MOE of the NC, miR-200b/a KD, and miR-200b/a + TET3 DKD mice ($n = 4$ mice each group; data represent the mean \pm SEM; Mash1: $F = 41.45$, Tuj1: $F = 113.9$, Cas3: $F = 92.51$, Ki67: $F = 61.35$, * $P < 0.05$, ** $P < 0.01$, *** $P < 0.001$, **** $P < 0.0001$; one-way ANOVA and Bonferroni pairwise comparisons).

The neuronal differentiation of cortical neural progenitor cells has been shown to be regulated by miR-15b through direct repression of TET3 (Lv *et al.*, 2014). In addition, studies on subsets of multipotent hematopoietic stem cells have demonstrated that miR-150-mediated TET3 is involved in classical monocyte differentiation (Selimoglu-Buet *et al.*, 2018). Although TET3 is highly expressed in the MOE (Colquitt *et al.*, 2013), the biological significance and the underlying mechanisms of TET3 in MOE development remain unclear. In this study, our data show that miR-200b/a uniquely regulates the expression of TET3 in the MOE. The defects caused by miR-200b/a knockdown can only be partially restored by inhibiting TET3 in the MOE, and we speculate that in addition to TET3, there may be other miR-200b/a target genes involved in the regulation of male behavior and cell phenotype in mice. Other miR-200b/a target genes may need to cooperate with TET3 to jointly regulate the male behaviors and the cell phenotypes of mice.

TET3 protein is predominantly cytoplasmic distributed in Mash1-marked GBCs of the NC mice (Fig 5J), consistent with its distributing in cytoplasm of neural precursor cells (Santiago *et al.*, 2020), whereas as products of TET3, 5mC and 5hmC are mainly located in the nuclei and express mostly to the OSN layers. Furthermore, no staining of 5hmC in the miR-200b/a KD mice is observed in basal MOE (Fig 5N), in line with previous studies that the 5hmC is mainly labeled with the post-mitotic neural cells (Globisch *et al.*, 2010; Szulwach *et al.*, 2011; Mellen *et al.*, 2012; Hahn *et al.*, 2013; Diotel *et al.*, 2017).

We further investigated how TET3 functions in the MOE to exert its effects. TET3 directly interacts with REST to facilitate derepression of REST target genes during post-natal retinal development (Perera *et al.*, 2015). Previous studies in the adult hippocampus have shown that REST plays a central role in neurogenesis (Ballas *et al.*, 2005; Nechiporuk *et al.*, 2016). Similar to the MOE, the neocortex is also composed of layers of neurons differentiated from their precursors. Overexpression of REST in the developing neocortex disturbed the spatiotemporal transition of neural stem/progenitor cells into neurons but not neuronal cell fate decisions (Mandel *et al.*, 2011). In addition, animals lacking both RCOR1 and RCOR2 or with INSM1 knockout in the developing brain are a phenocopy of our miR-200b/a KD mice, with increased number of neural progenitors but decreased numbers of neurons, concomitant with REST gene upregulation in these animals (Monaghan *et al.*, 2017).

The MOE is a relatively independent peripheral nerve organ, and whether olfactory neurogenesis in the MOE is also regulated by REST has not been reported. Herein, we presented the following: (i) The Co-IP data showed that TET3 and REST formed interaction complexes in the MOE; (ii) miR-200b/a knockdown-induced deficits in male aggressive and mating behavior and defects such as GBC proliferation and differentiation were restored by silencing REST expression. Because no binding site of miR-200b/a was found on the REST 3' UTR, our results strongly indicate that an increase in REST caused by miR-200b/a knockdown in the MOE is achieved by acting on TET3.

Because TET3 is a DNA demethylase, TET3 may regulate REST expression by altering the DNA methylation levels in the promoter. Our results showed that TET3 does not regulate REST expression at the transcriptional level. The interaction between TET3 and the thyroid hormone receptor (TR) is necessary to maintain the stability of the TR protein (Guan *et al.*, 2017). Therefore, we speculated that TET3 may also stabilize REST expression in a similar manner. In fact, Western blot analyses of NIH3T3 cells treated with cycloheximide (CHX, protein translation inhibitor), PYR-41 (ubiquitination degradation inhibitor), or Mg132 (proteasome degradation inhibitor) confirmed that TET3 improved the stability of the REST protein by inhibiting the degradation of the ubiquitinated proteasome (Fig EV2F–H). Nevertheless, to our knowledge, this is the first study to elucidate the role of REST in MOE olfactory neurogenesis.

REST exerts versatile functions by recruiting various cofactors to assemble a complex at the promoters of target genes and orchestrating epigenetic remodeling (Hwang & Zukin, 2018). These recruited cofactors vary based on cell type, tissue, spatiotemporal context, developmental stage, and gene context. Furthermore, the subset of genes bound by these cofactors varies in different cellular environments and at different ages (Sun *et al.*, 2005; Hwang *et al.*, 2017). In addition, the repertoire of REST-regulated genes can be reshaped by the abundance of genes that interact with REST, such as SF-1 (Doghman *et al.*, 2013). Nevertheless, REST has multiple roles, such as repressor, silencer, and activator, depending on the context of its expression (Chen *et al.*, 1998; Kallunki *et al.*, 1998; Kuwabara *et al.*, 2004; Abrajano *et al.*, 2010; Gao *et al.*, 2011). The final impact on transcriptional activity governed by the REST protein is dependent on the balance of these effects (Seth & Majzoub, 2001). Based on these preceding discussions, we

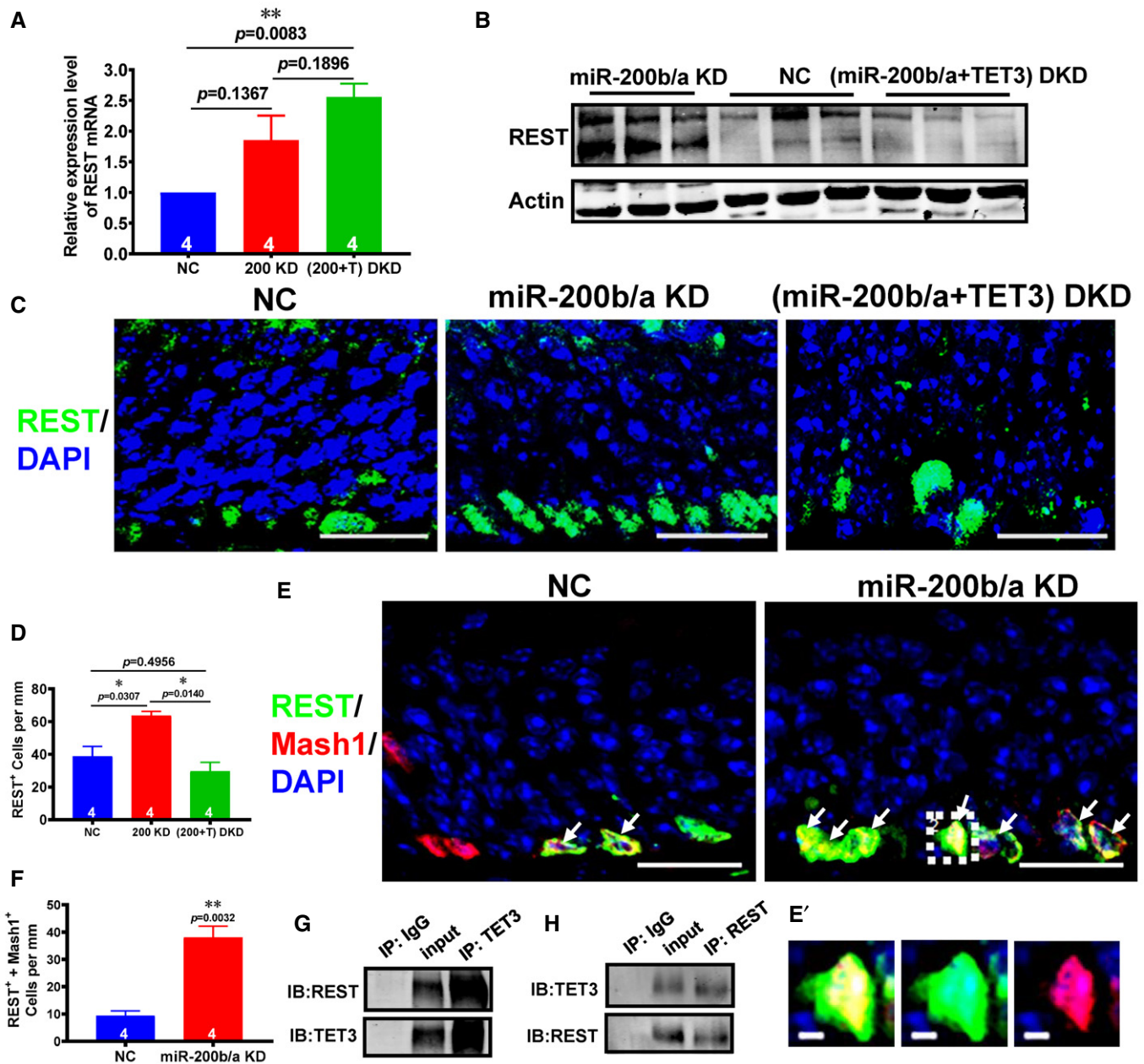


Figure 7. TET3 and REST interactions in the mouse MOE.

- A** The REST mRNA expression in the MOE of the NC, miR-200b/a KD, and miR-200b/a + TET3 DKD mice, as revealed by qPCR analysis (200 KD: miR-200b/a KD; [200 + T] DKD: [miR-200b/a + TET3] DKD; $n = 4$ mice each group; data represent the mean \pm SEM; $F = 9.409$, NC vs. 200: $P = 0.1367$, 200 vs. 200 + T: $P = 0.1896$, $**P < 0.01$; one-way ANOVA and Bonferroni pairwise comparisons).
- B** Western blot analysis of the REST protein level in the MOE of the NC, miR-200b/a KD and miR-200b/a + TET3 DKD mice ($n = 3$ mice each group). Actin served as a loading control.
- C** Representative IF staining for REST in the MOE of the NC, miR-200b/a KD, and miR-200b/a and TET3 DKD mice. Scale bars: 20 μ m.
- D** Quantification of the number of REST⁺ cells in the MOE of the NC, miR-200b/a KD, and miR-200b/a + TET3 DKD mice ($n = 4$ mice each group; data represent the mean \pm SEM; $F = 12.11$, $*P < 0.05$; one-way ANOVA and Bonferroni pairwise comparisons).
- E** Representative IF containing with REST and Mash1 antibodies in the MOE of the NC and miR-200b/a KD mice. The white arrows indicate the cells positive for both REST and Mash1. (E') are shown at higher magnification of the boxed region, as three-channel merged images (left image) and the separated channel (middle and right images). (E): Scale bars, 20 μ m; (E'): Scale bars, 2 μ m.
- F** Quantification of the number of co-stained REST⁺ and Mash1⁺ cells in the MOE of the NC and miR-200b/a KD mice ($n = 4$ mice each group; data represent the mean \pm SEM; $**P < 0.01$; Student's t -test).
- G** Mouse MOE proteins were immunoprecipitated with polyclonal antibodies against TET3. Input protein (100 μ g) and immunoprecipitates were subjected to immunoblot analysis with the indicated antibodies. IgG antibodies were used as the negative control.
- H** Mouse MOE proteins were immunoprecipitated with polyclonal antibodies against REST. Input protein (100 μ g) and immunoprecipitates were subjected to immunoblot analysis with the indicated antibodies. IgG antibodies were used as the negative control.

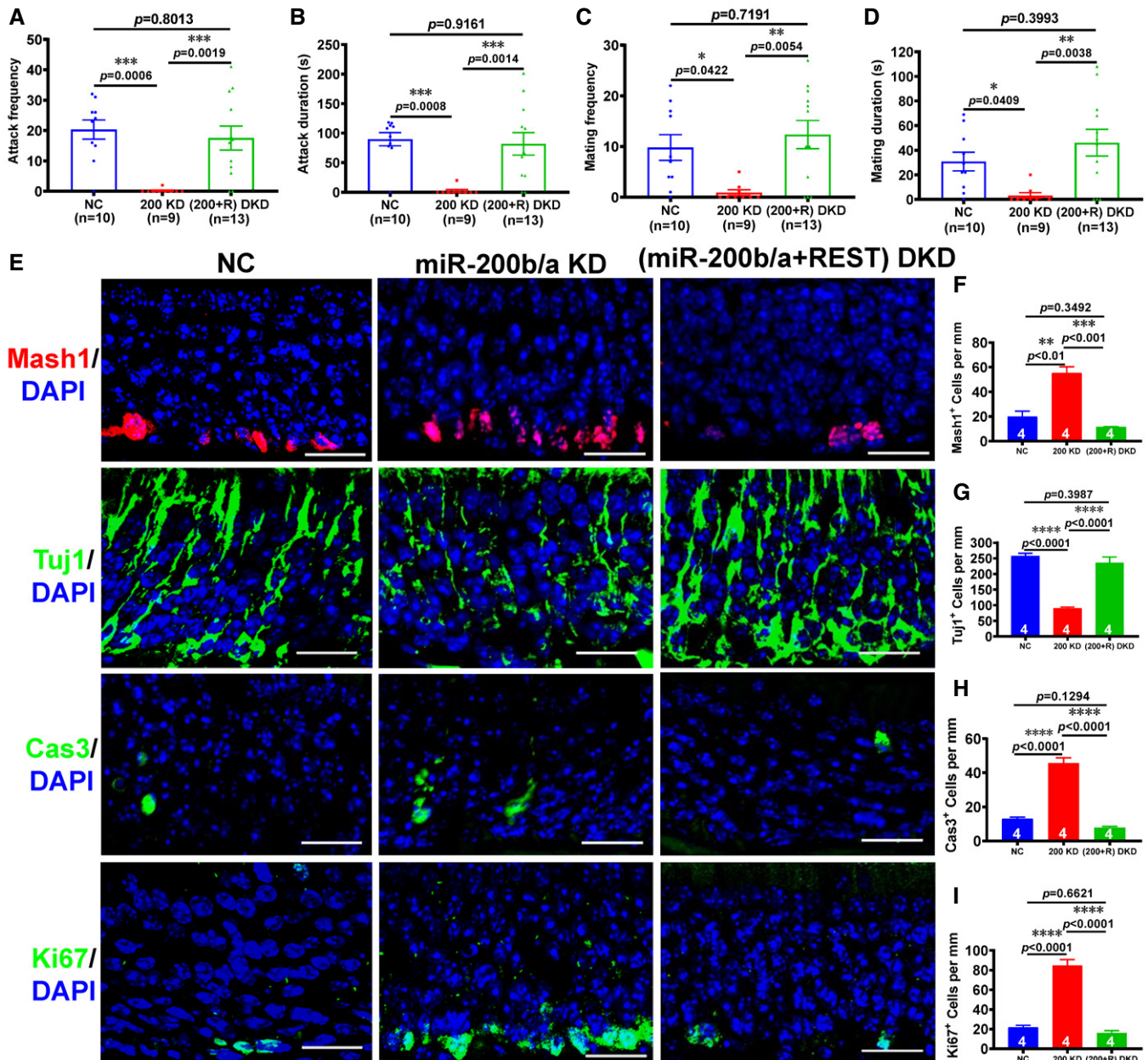


Figure 8. The miR-200b/a-induced deficits, including GBC proliferation and differentiation and male behaviors, are rescued by REST knockdown.

A, B The resident/intruder experiment showed that the attack frequency (A) and duration (B) of the miR-200b/a + REST DKD mice were dramatically improved compared with those of the miR-200b/a KD mice (200 KD: miR-200b/a KD; [200 + R] DKD: [miR-200b/a + REST] DKD; NC: $n = 10$ mice, miR-200b/a KD: $n = 9$ mice, miR-200b/a + REST DKD: $n = 13$ mice; data represent the mean \pm SEM; A: $F = 10.62$, B: $F = 10.54$, $***P < 0.001$; one-way ANOVA and Bonferroni pairwise comparisons).

C, D The analysis of male–female mating behaviors showed that the frequency (C) and duration (D) of mating to females of the miR-200b/a + REST DKD mice were significantly improved compared with those of the miR-200b/a KD mice (NC: $n = 10$ mice, miR-200b/a KD: $n = 9$ mice, miR-200b/a + REST DKD: $n = 13$ mice; data represent the mean \pm SEM; C: $F = 6.162$, D: $F = 6.360$, $*P < 0.05$, $**P < 0.01$; one-way ANOVA and Bonferroni pairwise comparisons).

E Representative IF staining for Mash1, Tuj1, Cas3, and Ki67 in the MOE of the NC, miR-200b/a KD, and miR-200b/a + REST DKD mice. Scale bars: 20 μ m.

F–I Quantification of the number of Mash1⁺ (F), Tuj1⁺ (G), Cas3⁺ (H), and Ki67⁺ (I) cells in the MOE of the NC, miR-200b/a KD, and miR-200b/a + REST DKD mice ($n = 4$ mice each group; data represent the mean \pm SEM; Mash1: $F = 35.53$, Tuj1: $F = 62.28$, Cas3: $F = 115.7$, Ki67: $F = 77.43$, $**P < 0.01$, $***P < 0.001$, $****P < 0.0001$; one-way ANOVA and Bonferroni pairwise comparisons).

postulate that the behavioral abnormalities and compromised olfactory neurogenesis exhibited in mice with miR-200b/a knockdown in the MOE could be caused by aberrant REST expression in the

GBCs at inappropriate times and/or developmental stages (Majumder, 2006) due to the elevated levels of TET3 induced by miR-200b/a knockdown in the MOE. These changes result in the

upregulation of proliferation-associated genes and the downregulation of differentiation-associated genes.

Alternatively, REST suppresses the expression of miRNAs (Hwang *et al*, 2014), especially miR-132, a well-known neuron-specific cAMP-response element binding protein (CREB)-regulated miRNA (Wu & Xie, 2006), and is specifically enriched in GBCs (Colquitt *et al*, 2013). Given that miR-132 is critical for the regulation of MeCP2 protein levels and Notch signals in neurons (Mendoza-Viveros *et al*, 2017; Engler *et al*, 2018), and both of these factors affect olfactory neurogenesis (Li *et al*, 2014; Dai *et al*, 2018; Herrick *et al*, 2018), a possible link between this molecule and the behavioral abnormalities and impaired olfactory neurogenesis in mice with miR-200b/a knockdown in the MOE could not be ruled out. Further studies are needed.

The MOE is a special physiological structure that is directly exposed to the external environment, which has made intranasal installation an attractive means of manipulating gene expression in the MOE. AAV not only avoids interfering with the function of adjacent genes and causes insertion mutations but also has few immune responses, shows effective infection of neurons (Williams *et al*, 2017), and can result in persistent expression in OSNs (Samulski *et al*, 1991). Given these findings, AAV has recently been used to infect mice with OSNs through nasal perfusion (Green *et al*, 2018). Our results demonstrated the feasibility of combined AAV packaging CRISPR-Cas9 with nasal perfusion technology for gene editing in the nasal cavity. The findings also suggest that a similar approach might be used for gene therapy of human olfactory-related diseases, as shown in approaches targeting the muscles (Bengtsson *et al*, 2017) and ears (György *et al*, 2019).

In conclusion, our study demonstrated that a miR-200b/a/TET3/REST regulatory axis at the right time and stage of development is critical for a balance between proliferation and neuronal differentiation of GBCs in the MOE, as well as olfactory-mediated behaviors. Because miR-200b/a, TET3, and REST are abundantly expressed in many other tissues, the mechanical insights made in this study should have broad implications beyond MOE tissue.

Materials and Methods

Animals

AC3^{+/+} and AC3^{-/-} mice were bred from AC3^{+/-} mice, and the genotype was authenticated as previously described (Wang & Storm, 2006). All mice used in this study were males at 3 months of age, unless indicated. The mice were housed under a 12-h light (07:00–19:00 h)/dark (19:00–07:00 h) cycle at 22°C and fed regular chow *ad libitum* in an SPF animal room. All experimental procedures used in the study were performed according to the Guiding Opinions on the Treatment of Experimental Animals issued by the Ministry of Science and Technology, People's Republic of China and approved by the Animal Ethics and Caring Committee of Hebei University (approval NO.: IACUC-2017013).

Cells

HeLa, 3T3-L1, and NIH3T3 cell lines were maintained in DMEM (Gibco) supplemented with 10% fetal bovine serum (Gibco) and 1%

penicillin/streptomycin (Gibco) in a 37°C incubator with a humidified 5% CO₂ atmosphere.

RNA isolation and qPCR analyses

MiRNAs were extracted using the miRNeasy Mini Kit (QIAGEN), and reverse translation was performed using a Mir-X miRNA First-Strand Synthesis Kit (Clontech). Expression of mature miR-200b and miR-200a was detected using NovaTM SYBR PCR Master Green mix (QIAGEN) and miR-200a and miR-200b qPCR primers (Table EV1). The snoRNA U6 was used for normalization. Total RNA was isolated using the RNeasy Micro Kit (QIAGEN), and first-strand cDNA was synthesized using a PrimeScriptTM RT reagent Kit with gDNA Eraser (TaKaRa). The expression of mRNAs was assessed with NovaTM SYBR Green PCR Master Green mix (QIAGEN), and analysis was performed using the 2^{-ΔΔC_T} method (Livak & Schmittgen, 2001). All qPCR samples were normalized to β-actin. The specific primers used for qPCR are listed in Table EV1.

Small RNA sequencing and RNA-seq analyses

Small RNA sequencing of the MOE from adult (3-month-old) male wild-type mice ($n = 2$) and AC3 knockout mice ($n = 2$) was performed by Novogene (Beijing, China). Sequencing libraries were generated using a NEBNext[®] Multiplex Small RNA Library Prep Set for Illumina[®] (NEB) following the manufacturer's recommendations. The library preparations were sequenced on an Illumina HiSeq 2500/2000 platform, and 50 bp single-end reads were generated. The original data (raw reads) were processed through custom Perl and Python scripts. Differential expression analysis was performed using the DESeq R package (1.8.3).

RNA sequencing analysis of the whole MOE from adult male NC mice ($n = 3$) and miR-200b/a KD mice ($n = 3$) was performed by Annoroad Co. (Beijing, China). Sequencing libraries were generated using the NEBNext[®] UltraTM RNA Library Prep Kit for Illumina[®] (NEB) following the manufacturer's recommendations. The libraries were sequenced on an Illumina platform, and 150 bp paired-end reads were generated. The original data (raw reads) were filtered using Perl script, and DESeq2 was used to estimate the expression level of each gene in each sample. The P -value was calculated by the Wald test and corrected by the BH method. Genes with $q \leq 0.05$ were identified as significantly differentially expressed genes (DEGs).

DNA editing assay of guide RNAs in 3T3-L1 cells

gRNAs targeting the miR-200b/a cluster were designed using an online tool (CRISPR, <http://crispr.mit.edu>). Four or five gRNAs at each site were chosen and synthesized by BGI (Beijing, China). These gRNAs were cloned into the BbsI site of pSpCas9 (BB)-2A-Puro (pX459, Addgene) and validated by Sanger sequencing. For functional testing of sgRNAs, 70–90% confluent 3T3-L1 cells were transfected with the pX459 + sgRNA recombinant plasmid. Cells transfected with pX459 only were served as negative controls. Puromycin screening was performed after transfection for 24 h. Genomic DNA (gDNA) was extracted from transferred cells after puromycin screening using Quick Extract DNA extraction solution (Epizentre) according to the manufacturer's instructions. To determine the

targeting efficiency, individual sgRNAs were assessed using the EnGen[®] Mutation Detection Kit (NEB). gDNA was used as a template for PCR using Q5 high-fidelity DNA polymerases (NEB). PCR products were digested by T7 Endonuclease I (NEB). The cleavage intensity was quantified using ImageJ. The indel efficiency was estimated according to Ran *et al* (2013). The optimal gRNA for each site, whose indel efficiency was the highest, was used in the following studies. The sequences for gRNAs and shRNA include miR-200b/a cluster F' guide RNA (5'-GGAAGTCCCCGGTCCGAGG-3'), miR-200b/a cluster R' guide RNA (5'-GCCTGTCTTCGGCGAATGG T-3'), TET3 guide RNA (5'-GCTCCAACGAGAAGCTATTG-3'), and REST shRNA (5'-GCCGAATCTGAAGAGCAGT-3'). The PCR primers are listed in Table EV1.

Production of AAV vectors

For the spCas9 AAV vector, the spCAS9 sequence was obtained by PCR. pMecp2, NLS, and spA were chemically synthesized. All fragments were ligated using the Golden Gate cloning strategy. Then, pMecp2-NLS-spCAS9-NLS-spA was cloned into the AAV backbone. For miR-200b/a sgRNA AAV, the PCR-amplified hU6 promoter was ligated with miR-200a and miR-200b sgRNAs using the Golden Gate assembly method. The ligation fragment, including two single gRNAs and the U6 promoter, was cloned into the AAV backbone. For TET3 sgRNA or REST shRNA, the fragment was ligated with a PCR-amplified hU6 promoter using the Golden Gate assembly method. The ligation fragments (containing TET3 sgRNA or REST shRNA and U6 promoter) were cloned into the AAV backbone. LacZ sgRNA, as the negative control, was cloned alone into the AAV backbone. The sequences of all obtained constructs were validated by further Sanger sequencing. Then, these AAVs were packaged by Hanbio (Shanghai, China).

Intranasal delivery of AAV vectors or mimic for transduction of the MOE

For the NC and miR-200b/a KD mice, 3 μ l of a 1:1 AAV mixture (1.1×10^{12} vector genomes [Vg]/ml of SpCas9 + 1.1×10^{12} Vg/ml of NC sgRNA or 1.1×10^{12} Vg/ml of miR-200b/a cluster sgRNAs) was diluted into 17 μ l of normal saline (each nostril). For miR-200b/a + TET3 DKD mice, 6 μ l of a 1:1:2 AAV mixture (1.1×10^{12} Vg/ml of SpCas9 + 1.1×10^{12} Vg/ml of miR-200b/a cluster sgRNAs + 1.1×10^{12} Vg/ml of TET3 sgRNA) was diluted into 14 μ l of normal saline (each nostril). For all experiments with intranasal AAV vector delivery, the mice (4–6 weeks old) were lightly anesthetized with isoflurane, and viral delivery was performed by a 0.5–10 μ l pipettor placed at the nostrils and administered during each inhalation. A 20 μ l dose of AAV (10 μ l each time) was slowly perfused into each nostril. The subsequent experiments were performed 8 weeks later. For the miR-200b/a + REST DKD mice, Cas9 and miR-200b/a sgRNA AAV mix were perfused into the nostril. The intranasal delivery procedure was the same as that in the miR-200b/a KD mice. After 5 weeks, REST shRNA AAV (3 μ l of AAV in 17 μ l of normal saline in each nostril) was reperfused into the nostril of the above mice. The subsequent experiments were performed 3 weeks later.

For miR-200b and miR-200a mimic, 5 μ g of mimic and 1 μ l of Lipo3000 (Thermo Scientific) were diluted into 20 μ l of DEPC H₂O

(each nostril). The mixture was perfused into the nostril of adult mice. The intranasal delivery procedure was similar to that described for AAV injection. The subsequent experiments were performed 1 week later.

Western blot assays

RIPA Lysis and Extraction Buffer (Pierce) was used to extract protein from MOE tissues or cells. The protein concentration was determined using the BCA method. We separated the proteins (equal amounts of each sample) by SDS–polyacrylamide gel electrophoresis and then transferred them to Immobilon-P[®] Transfer Membranes (Millipore). The membrane was incubated in a blocking solution (5% nonfat dry milk in TBS) at room temperature (RT) for 1–2 h. The primary antibody (including Sox2 [1:500; Abcam; Catalogue # ab97959], Mash1 [1:500; BD Biosciences; Catalogue # 556604], TET3 [1:500; Abcam; Catalogue # ab139805], TET1 [1:500; Abcam; Catalogue # ab191698], REST [1:500; Merck Millipore; Catalogue # 07-579], Actin [1:2,000; Proteintech; Catalogue # 60009-1-1g], GAPDH [1:2,000; Proteintech; Catalogue # 60004-1-1g], and Tubulin [1:1,000; Sigma; Catalogue # T9026]) was incubated at 4°C overnight or at RT for 2–3 h. Secondary antibody (conjugated with 680 or 800 nm fluorophores, SeraCare KPL, 1:10,000 in TBST buffer) was incubated for 1 h at RT. Images were obtained using Odyssey software (Li-Cor). The gray value of the protein of interest was quantified by ImageJ, and the relative expression level of the protein was estimated as the gray value of the protein of interest/the gray value of the loading control. Actin/GAPDH/Tubulin was used as loading controls.

Off-target sequence analysis

Off-target sites for the miR-200b/a cluster were predicted using CRISPOR (see URLs) (Haeussler *et al*, 2016), and the top 10 sites ranked by the mitOfftarget Score were subjected to next-generation sequencing (NGS). Dataset EV2 lists the predicted miR-200b/a off-target sites, which were used for off-target NGS analysis. PCR amplicons of predicted off-target sites were subjected to NGS. We determined off-target base editing proportions and indel proportions using data from NGS. Briefly, adaptor sequences, PCR primers, bases of quality under 20, and sequences with *N* bases above 10% were removed by Cutadapt. The clean data were aligned with the reference genome by BWA, and duplications were removed in the results by Picard. Samtools were used to analyze InDel, and the variants were annotated by Annovar.

Behavior tests

For behavior tests, the mice, which were perfused with AAV at the indicated time, were habituated to the experimenter 7 days before behavioral testing for acclimation. The experimenter did not know the genotype of each mouse on the behavioral testing day.

Locomotor activity was measured by the open field test for 10 min using an Opto-Varimetric-3 sensor system (Columbus Instruments). The activity time was recorded.

The olfactory habituation assay was performed as described previously (Trinh & Storm, 2003). In brief, the mice whose nostrils were perfused with AAV were individually housed for 5 days with

access to water and food. During the experiment, the mice were exposed to a cotton swab with water for 120 s, and the frequency of sniffs was recorded. This experiment was conducted twice. Then, an odorant-soaked cotton swab was presented. The frequency of sniffs of the cotton swab laced with an odorant was recorded for 120 s. This test was conducted two times with 60 s between trials, followed by the introduction of the other odorant. These odorants included male urine (1:50), female urine (1:50), isopentyl acetate (50 μ M), citral (50 μ M), 2-heptanone (50 μ M), and propyl propionate (50 μ M). The data are shown as a ratio of the frequency of sniffs a mouse took when the cotton swab with the odorant was initially presented to the frequency of sniffs observed when the swab with water was initially presented.

Male–male aggression was tested by the resident/intruder experiment (Leypold *et al*, 2002). In brief, the experimental animals were housed alone for 15 days with water and food *ad libitum*, and their bedding was not changed for the 7 days prior to testing. On the test day, a group-housed, adult, unfamiliar, sexually inexperienced, wild-type male mouse was introduced into the home cage of the experimental mice during a 15-min period. The attack frequency and duration of the experimental mice were recorded. Attack behavior was defined as wrestling/tumbling, biting, and chasing. Male–female mating behaviors of experimental mice were monitored over a 15-min period by placing an unfamiliar, sexually receptive, adult, wild-type female mouse into the home cage of the resident male mice. The mounting frequency and duration were recorded.

BrdU and EdU lineage tracing

For analysis of cell cycle exit, male mice (NC and miR-200b/a KD, $n = 4$ mice each group, 12–14 weeks old) were intraperitoneally injected with EdU (Sigma; 50 mg/kg body weight, dissolved in sterile saline). Tissues were collected 24 h after injection. For analysis of the length of the S phase, male mice (NC and miR-200 KD, $n = 3$ mice each group, 12–14 weeks old) were intraperitoneally injected with BrdU. After 3 h, the above mice were intraperitoneally injected with EdU. For analysis of the total length of the cell cycle, male mice (NC and miR-200 KD, $n = 3$ mice each group, 12–14 weeks old) were intraperitoneally injected with BrdU. After 20 h, the above mice were intraperitoneally injected with EdU. Tissues were collected 45 min after the EdU injection (Brandt *et al*, 2012). For analysis of differentiation of GBCs, male mice (NC and miR-200 KD, $n = 3$ mice each group, 12–14 weeks old) were injected with BrdU twice (with intervals of 2 h). Tissues were collected 3 days after BrdU injection (Liberia *et al*, 2019).

MOE tissue processing and IF

The MOE tissue was fixed in 4% paraformaldehyde (PFA) solution. After 24 h, MOE tissue was washed with PBS, decalcified in 10% EGTA in PBS for at least 5 days, and dehydrated using 30% sucrose until the tissue was completely covered. The MOE tissue was embedded in OCT medium (SAKURA) and cut into 10- μ m-thick sections using a cryostat. For IF, tissue sections were washed for 5 min with PBS, fixed for 20 min in 4% PFA solution, permeabilized for 30 min with 0.5% Triton X-100 in PBS, blocked with blocking solution (PBS supplemented with 0.01% Triton X-100, 10% normal donkey/goat serum, 5% non fat dry milk and 4% bovine

serum albumin) for 1 h, and then incubated in primary antibody solution (specific antibody in blocking solution) for 16 h at 4°C. We used primary antibodies to the following antigens: Cas9 (1:500; Rabbit; Rockland; Catalogue # 600-401-GK0; for costaining with Cas9 and OMP), Cas9 (1:500; Mouse; Epigentek; Catalogue # A-9000; for other IF), Ki67 (1:200; Abcam; Catalogue # ab15580), CK14 (1:1,000; Thermo Scientific; Catalogue # PA5-28002), Sox2 (1:500; Abcam; Catalogue # ab97959), Tuj1 (1:500; Abcam; Catalogue # ab18207), GAP43 (1:500; Merck Millipore; Catalogue # AB5220), OMP (1:500; Wako; Catalogue # 019-22291), Cas3 (1:200; Cell Signaling Technology; Catalogue # 9661), Foxg1 (1:500; Abcam; Catalogue # ab18259), TET3 (1:500; Abcam; Catalogue # ab139805), 5mC (1:500; Cell Signaling Technology; Catalogue # 28692), 5hmC (1:500; active motif; Catalogue # 39791), and REST (1:500; Merck Millipore; Catalogue # 07-579). The secondary antibodies (Alexa 488-, 594-, or 568-conjugated; 1:500; Thermo Scientific) were incubated for 2 h at RT, followed by nuclear counterstaining with DAPI (Sigma). After each step, the sections were carefully washed in PBS. The EdU signals were measured by the EdU Click-iT reaction (Thermo Scientific). Fluorescent confocal slices were obtained using an Olympus FLUOVIEW FV3000 confocal microscope.

For tissue sections immunostained for Mash1 (1:200; Rabbit; Abcam; Catalogue # ab74065 or 1:200; Mouse; BD Biosciences; Catalogue # AF796, for Mash1/TET3 costaining and Mash1/REST costaining), antigen retrieval and the tyramide signal amplification (TSA) method (Wang *et al*, 1999) were necessary. In brief, the sections were incubated in 0.01 M citrate buffer at pH 6 and at 95°C for 15 min and then cooled for 30 min at RT. For signal detection, an HRP-labeled secondary antibody (1:1,000; Proteintech) was used to replace the Alexa 488- or 594-conjugated secondary antibody. Signal detection was performed using TSA™ Fluorescence Systems (PerkinElmer, Catalogue # NEL701A001KT) following the manufacturer's guidelines. Other experimental steps were the same as above.

For BrdU and GAP43 costaining, the sections were thawed at 37°C and treated for antigen retrieval with 0.01 M citrate buffer at pH 6 and 70°C for 30 min. Those sections were also treated with 2 N HCl at 37°C for 20 min for DNA denature. Then, they were incubated in a blocking solution (PBS supplemented with 0.1% Triton X-100, 5% normal donkey serum, and 0.1% bovine serum albumin) for 1 h at RT. Then, sections were incubated in a mixture of BrdU antibody (1:200; Abcam; Catalogue # ab6326) and GAP43 antibody (1:1,000; Merck Millipore; Catalogue # AB5220) diluted in PBS with 10% blocking solution at 4°C overnight, followed by incubation with secondary antibodies (Alexa 488- and 568-conjugated; 1:500; Thermo Scientific) diluted in PBS for 2 h at RT. Nuclei were counterstained by incubating the section with DAPI. After each step, the sections were carefully washed in PBS.

Cell cycle exit and the length of the S phase and total cell cycle analysis

The cell cycle exit index was measured by the EdU Click-iT reaction (Thermo Scientific) and Ki67 IF. Under the above conditions, cells that exited the cell cycle after injection of EdU were EdU⁺ and Ki67⁻ and cells that were still cycling were EdU⁺ and Ki67⁺. The cell cycle exit index was calculated as follows: (EdU⁺ Ki67⁻ cells/total EdU⁺ cells) \times 100. The length of the S phase and total cell cycle was measured by the EdU Click-iT reaction and BrdU IF. The

length of the S phase (T_s) and total cell cycle (T_c) was calculated as follows: $T_s = 3 \text{ h} \times \text{BrdU}^+/\text{BrdU}^+\text{Edu}^-$; $T_c = 20 \text{ h} + (T_s \times \text{Edu}^+/\text{BrdU}^-/\text{Edu}^+)$ (Brandt *et al*, 2012).

Imaging and quantitative analysis for IF

All images were acquired under the same conditions (eight evenly spaced sections per mouse through the anterior to posterior epithelium were counted in the four animals per group) and processed identically. Image J and Photoshop CC software were used to process the images. AxioVision software was used to measure the epithelial length along the olfactory mucosa. The images were analyzed by an experimenter who was blinded to the treatment of each sample. The representative regions of MOE were used to calculate cell density appropriate for 10- μm -thick sections according to the Abercrombie method (Abercrombie, 1946). Immunopositive cell density was calculated by the number of immunopositive cells/epithelial length (cells number/mm) for each group. The final number of immunoreactive cells was transformed according to the following formula: corrected number = immunoreactive cells number \times (slice thickness/[average nucleus size + slice thickness]) (Abercrombie, 1946).

The target genes of miR-200 and luciferase assays

The online target prediction database TargetScan (<http://targetscan.org>) was used to identify the putative targeting genes of miR-200b and miR-200a. The sequence for the mouse TET3 transcript (NM_030693; ENST00000423777.2) was searched in GenBank and the UCSC Genome Browser. Information on miR-200a (MI0000554) and miR-200b (MI0000243) was acquired from miRBase.

For construction of the luciferase reporters, a partial TET3 3' UTR, including the miR-200a potential targeting site, was amplified by PCR from gDNA of mouse tissue. The DNA fragment was cloned in the pmirGLO Dual-Luciferase Vector (Promega). The Mut Express α Fast Mutagenesis Kit V2 (Vazyme) was used to perform targeted mutagenesis of the miR-200a potential binding site of the TET3 3' UTR. The primers of the plasmid constructs are listed in Table EV1. HeLa cells were cotransfected with the dual-luciferase plasmid containing WT TET3 3' UTR or Mut TET3 3' UTR and miR-200a mimic or nontargeting NC oligos and cultured for 48 h before the luciferase assay. Firefly and Renilla luciferase activities were detected with a dual-luciferase reporter assay system (Promega), and the results are shown as firefly luciferase activity relative to Renilla luciferase activity.

Transient transfection with oligonucleotides

For oligonucleotides, 100 nM of miR-200a mimic or nontargeting NC oligos or 50 nM of miR-200a inhibitor or NC inhibitor was transfected into 3T3-L1 cells using HiPerFect Transfection Reagent (QIAGEN). The transfected cells were harvested after transfection for 48 h (for mRNA studies) or 72 h (for protein studies).

Co-IP

Protein from MOE tissues was isolated in immunoprecipitation buffer containing protease and phosphatase inhibitor cocktail (Cell Signaling Technology). The protein lysates were precleared with

Mouse IgG (Sepharose[®] Bead Conjugate; Cell Signaling Technology; Catalogue # 2729) and immunoprecipitated with constant rotation at 4°C for 16 h using 5 μg of the anti-TET3 primary antibody [C3], anti-REST primary antibody, or normal rabbit IgG, followed by 4 h of incubation with mouse IgG. The samples were washed at least five times on ice using immunoprecipitation buffer with permanent rotation, and then, the beads were resuspended in 2 \times SDS loading buffer by boiling and analyzed by Western blot.

REST protein stability assay

NIH3T3 cells were transfected with 20 nM TET3 siRNA or nontargeting NC oligos using the Lipo3000 Transfection Reagent. The transfected cells were combined with PYR-41 (5 μM), Mg132 (10 μM), CHX (20 $\mu\text{g}/\text{ml}$), or dimethyl sulfoxide (DMSO; as the negative control) after culturing for 48 h. Transfected cells treated with CHX (after culturing for 0, 2, 4, 8 h), PYR-41 (after culturing for 12 h), or Mg132 (after culturing for 12 h) were harvested, and the protein was extracted. The TET3 and REST levels in the above cells were analyzed by Western blot using anti-TET3 or anti-REST antibodies.

Statistical analysis

The statistical comparisons were performed on data originating from at least three biologically independent experimental replicates (as indicated in the figure legends). GraphPad Prism and SPSS 21.0 software were used to conduct the statistical comparisons. For comparisons between two treatment groups, a Student *t*-test was used. For comparisons among three or more treatment groups, one-way ANOVA followed by Bonferroni multiple comparison tests was used. The results are shown as the mean \pm standard error of the mean (SEM). **P*-values lower than 0.05 were considered statistically significant. For $n = 2$ mice or on technical replicates, the scatter blots were used.

Data availability

RNA-seq and small RNA-seq data have been deposited in GEO: GSE134554 (link: <https://www.ncbi.nlm.nih.gov/geo/query/acc.cgi?acc=GSE134554>) and GSE134468 (link: <https://www.ncbi.nlm.nih.gov/geo/query/acc.cgi?acc=GSE134468>).

Expanded View for this article is available online.

Acknowledgements

We thank Mingshen Guo for technical assistance with the imaging and Hongxin Zhang and Haichen Lian for routine animal husbandry. This work was supported by the National Natural Science Foundation of China (31871246 and 31471178), Institute of Life Science and Green Development, Hebei University (050001-5000019), the Excellent PhD Training Project of Hebei University to Dong Yang (20151975), and the Post-Graduate's Innovation Fund Project of Hebei University (hbu2018bs14) to Dong Yang.

Author contributions

Conceptualization: DY, ZW; Investigation: DY, XW, YZ, WW; Writing, review & editing: DY, ZW; Supervision: ZW; Project administration & funding acquisition: ZW.

Conflict of interest

The authors declare that they have no conflict of interest.

References

- Abercrombie M (1946) Estimation of nuclear population from microtome sections. *Anat Rec* 94: 239–247
- Abrajano JJ, Qureshi IA, Gokhan S, Molero AE, Zheng D, Bergman A, Mehler MF (2010) Corepressor for element-1-silencing transcription factor preferentially mediates gene networks underlying neural stem cell fate decisions. *Proc Natl Acad Sci USA* 107: 16685–16690
- Ballas N, Grunseich C, Lu DD, Speh JC, Mandel G (2005) REST and its corepressors mediate plasticity of neuronal gene chromatin throughout neurogenesis. *Cell* 121: 645–657
- Bartel DP (2009) MicroRNAs: target recognition and regulatory functions. *Cell* 136: 215–233
- Beites CL, Kawachi S, Crocker CE, Calof AL (2005) Identification and molecular regulation of neural stem cells in the olfactory epithelium. *Exp Cell Res* 306: 309–316
- Belgardt BF, Ahmed K, Spranger M, Latreille M, Denzler R, Kondratiuk N, von Meyenn F, Villena FN, Herrmanns K, Bosco D et al (2015) The microRNA-200 family regulates pancreatic beta cell survival in type 2 diabetes. *Nat Med* 21: 619–627
- Belluscio L, Gold GH, Nemes A, Axel R (1998) Mice deficient in G(olf) are anosmic. *Neuron* 20: 69–81
- Bengtsson NE, Hall JK, Odom GL, Phelps MP, Andrus CR, Hawkins RD, Hauschka SD, Chamberlain JR, Chamberlain JS (2017) Muscle-specific CRISPR/Cas9 dystrophin gene editing ameliorates pathophysiology in a mouse model for Duchenne muscular dystrophy. *Nat Commun* 8: 14454
- Brabletz S, Brabletz T (2010) The ZEB/miR-200 feedback loop—a motor of cellular plasticity in development and cancer? *EMBO Rep* 11: 670–677
- Brandt MD, Hübner M, Storch A (2012) Brief report: adult hippocampal precursor cells shorten S-phase and total cell cycle length during neuronal differentiation. *Stem Cells* 30: 2843–2847
- Brunet LJ, Gold GH, Ngai J (1996) General anosmia caused by a targeted disruption of the mouse olfactory cyclic nucleotide-gated cation channel. *Neuron* 17: 681–693
- Caggiano M, Kauer JS, Hunter DD (1994) Globose basal cells are neuronal progenitors in the olfactory epithelium: a lineage analysis using a replication-incompetent retrovirus. *Neuron* 13: 339–352
- Cai Y, Cheng T, Yao Y, Li X, Ma Y, Li L, Zhao H, Bao J, Zhang M, Qiu Z et al (2019) *In vivo* genome editing rescues photoreceptor degeneration via a Cas9/RecA-mediated homology-directed repair pathway. *Sci Adv* 5: eaav3335
- Chadderton N, Millington-Ward S, Palfi A, O'Reilly M, Tuohy G, Humphries MM, Li T, Humphries P, Kenna PF, Farrar GJ (2009) Improved retinal function in a mouse model of dominant retinitis pigmentosa following AAV-delivered gene therapy. *Mol Ther* 17: 593–599
- Chen ZF, Paquette AJ, Anderson DJ (1998) NRSF/REST is required *in vivo* for repression of multiple neuronal target genes during embryogenesis. *Nat Genet* 20: 136–142
- Choi PS, Zakhary L, Choi WY, Caron S, Alvarez-Saavedra E, Miska EA, McManus M, Harfe B, Giraldez AJ, Horvitz HR et al (2008) Members of the miRNA-200 family regulate olfactory neurogenesis. *Neuron* 57: 41–55
- Coleman JH, Lin B, Schwob JE (2017) Dissecting LSD1-dependent neuronal maturation in the olfactory epithelium. *J Comp Neurol* 525: 3391–3413
- Colquitt BM, Allen WE, Barnea G, Lomvardas S (2013) Alteration of genic 5-hydroxymethylcytosine patterning in olfactory neurons correlates with changes in gene expression and cell identity. *Proc Natl Acad Sci USA* 110: 14682–14687
- Cramer T, Rosenberg T, Kisliouk T, Meiri N (2019) Early-life epigenetic changes along the corticotropin-releasing hormone (CRH) gene influence resilience or vulnerability to heat stress later in life. *Mol Psychiatry* 24: 1013–1026
- Dai Q, Duan C, Ren W, Li F, Zheng Q, Wang L, Li W, Lu X, Ni W, Zhang Y et al (2018) Notch signaling regulates Lgr5(+) olfactory epithelium progenitor/stem cell turnover and mediates recovery of lesioned olfactory epithelium in mouse model. *Stem Cells* 36: 1259–1272
- Dehay C, Kennedy H (2007) Cell-cycle control and cortical development. *Nat Rev Neurosci* 8: 438–450
- Diotel N, Merot Y, Coumilleau P, Gueguen MM, Serandour AA, Salbert G, Kah O (2017) 5-hydroxymethylcytosine marks postmitotic neural cells in the adult and developing vertebrate central nervous system. *J Comp Neurol* 525: 478–497
- Doghman M, Figueiredo BC, Volante M, Papotti M, Lalli E (2013) Integrative analysis of SF-1 transcription factor dosage impact on genome-wide binding and gene expression regulation. *Nucleic Acids Res* 41: 8896–8907
- Dulac C, Torello AT (2003) Molecular detection of pheromone signals in mammals: from genes to behaviour. *Nat Rev Neurosci* 4: 551–562
- Engler A, Rolando C, Giachino C, Saotome I, Erni A, Brien C, Zhang R, Zimmer-Strobl U, Radtke F, Artavanis-Tsakonas S et al (2018) Notch2 signaling maintains NSC quiescence in the murine ventricular-subventricular zone. *Cell Rep* 22: 992–1002
- Fan J, Jia L, Li Y, Ebrahim S, May-Simera H, Wood A, Morell RJ, Liu P, Lei J, Kachar B et al (2017) Maturation arrest in early postnatal sensory receptors by deletion of the miR-183/96/182 cluster in mouse. *Proc Natl Acad Sci USA* 114: E4271–E4280
- Fletcher RB, Das D, Gadye L, Street KN, Baudhuin A, Wagner A, Cole MB, Flores Q, Choi YG, Yosef N et al (2017) Deconstructing olfactory stem cell trajectories at single-cell resolution. *Cell Stem Cell* 20: 817–830
- Foust KD, Salazar DL, Likhite S, Ferraiuolo L, Ditsworth D, Ilieva H, Meyer K, Schmelzer L, Braun L, Cleveland DW et al (2013) Therapeutic AAV9-mediated suppression of mutant SOD1 slows disease progression and extends survival in models of inherited ALS. *Mol Ther* 21: 2148–2159
- Gadye L, Das D, Sanchez MA, Street K, Baudhuin A, Wagner A, Cole MB, Choi YG, Yosef N, Purdom E et al (2017) Injury activates transient olfactory stem cell states with diverse lineage capacities. *Cell Stem Cell* 21: 775–790
- Gao Z, Ure K, Ding P, Nashaat M, Yuan L, Ma J, Hammer RE, Hsieh J (2011) The master negative regulator REST/NRSF controls adult neurogenesis by restraining the neurogenic program in quiescent stem cells. *J Neurosci* 31: 9772–9786
- Garaffo G, Conte D, Provero P, Tomaiuolo D, Luo Z, Pincioli P, Peano C, D'Atri I, Gitton Y, Etzion T, et al (2015) The Dlx5 and Foxg1 transcription factors, linked via miRNA-9 and -200, are required for the development of the olfactory and GnRH system. *Mol Cell Neurosci* 68: 103–119
- Gill JG, Langer EM, Lindsley RC, Cai M, Murphy TL, Murphy KM (2012) Snail promotes the cell-autonomous generation of Flk1(+) endothelial cells through the repression of the microRNA-200 family. *Stem Cells Dev* 21: 167–176
- Globisch D, Munzel M, Muller M, Michalakos S, Wagner M, Koch S, Bruckl T, Biel M, Carell T (2010) Tissue distribution of 5-hydroxymethylcytosine and search for active demethylation intermediates. *PLoS ONE* 5: e15367
- Green WW, Uytengco CR, Ukhanov K, Kolb Z, Moretta J, McIntyre JC, Martens JR (2018) Peripheral gene therapeutic rescue of an olfactory ciliopathy

- restores sensory input, axonal pathfinding, and odor-guided behavior. *J Neurosci* 38: 7462–7475
- Guan W, Guyot R, Samarut J, Flamant F, Wong J, Gauthier KC (2017) Methylcytosine dioxygenase TET3 interacts with thyroid hormone nuclear receptors and stabilizes their association to chromatin. *Proc Natl Acad Sci USA* 114: 8229–8234
- György B, Nist-Lund C, Pan B, Asai Y, Karavitaki KD, Kleinstiver BP, Garcia SP, Zaborowski MP, Solanes P, Spataro S et al (2019) Allele-specific gene editing prevents deafness in a model of dominant progressive hearing loss. *Nat Med* 25: 1123–1130
- Haeussler M, Schonig K, Eckert H, Eschstruth A, Mianne J, Renaud JB, Schneider-Maunoury S, Shkumatava A, Teboul L, Kent J et al (2016) Evaluation of off-target and on-target scoring algorithms and integration into the guide RNA selection tool CRISPOR. *Genome Biol* 17: 148
- Hahn MA, Qiu R, Wu X, Li AX, Zhang H, Wang J, Jui J, Jin SG, Jiang Y, Pfeifer GP et al (2013) Dynamics of 5-hydroxymethylcytosine and chromatin marks in mammalian neurogenesis. *Cell Rep* 3: 291–300
- Hansen A, Zeiske E (1998) The peripheral olfactory organ of the zebrafish, *Danio rerio*: an ultrastructural study. *Chem Senses* 23: 39–48
- Hasuwa H, Ueda J, Ikawa M, Okabe M (2013) miR-200b and miR-429 function in mouse ovulation and are essential for female fertility. *Science* 341: 71–73
- Herrick DB, Guo Z, Jang W, Schnittke N, Schwob JE (2018) Canonical notch signaling directs the fate of differentiating neurocompetent progenitors in the mammalian olfactory epithelium. *J Neurosci* 38: 5022–5037
- Hoefert JE, Bjerke GA, Wang D, Yi R (2018) The microRNA-200 family coordinately regulates cell adhesion and proliferation in hair morphogenesis. *J Cell Biol* 217: 2185–2204
- Horlbeck MA, Witkowsky LB, Guglielmi B, Replogle JM, Gilbert LA, Villalta JE, Torigoe SE, Tjian R, Weissman JS (2016) Nucleosomes impede Cas9 access to DNA *in vivo* and *in vitro*. *Elife* 5: e12677
- Huard JM, Schwob JE (1995) Cell cycle of globose basal cells in rat olfactory epithelium. *Dev Dyn* 203: 17–26
- Hwang JY, Kaneko N, Noh KM, Pontarelli F, Zukin RS (2014) The gene silencing transcription factor REST represses miR-132 expression in hippocampal neurons destined to die. *J Mol Biol* 426: 3454–3466
- Hwang JY, Aromolaran KA, Zukin RS (2017) The emerging field of epigenetics in neurodegeneration and neuroprotection. *Nat Rev Neurosci* 18: 347–361
- Hwang JY, Zukin RS (2018) REST, a master transcriptional regulator in neurodegenerative disease. *Curr Opin Neurobiol* 48: 193–200
- Isaac RS, Jiang F, Doudna JA, Lim WA, Narlikar GJ, Almeida R (2016) Nucleosome breathing and remodeling constrain CRISPR-Cas9 function. *Elife* 5: e13450
- Ito S, D'Alessio AC, Taranova OV, Hong K, Sowers LC, Zhang Y (2010) Role of Tet proteins in 5mC to 5hmC conversion, ES-cell self-renewal and inner cell mass specification. *Nature* 466: 1129–1133
- Iwema CL, Schwob JE (2003) Odorant receptor expression as a function of neuronal maturity in the adult rodent olfactory system. *J Comp Neurol* 459: 209–222
- Kallunki P, Edelman GM, Jones FS (1998) The neural restrictive silencer element can act as both a repressor and enhancer of L1 cell adhesion molecule gene expression during postnatal development. *Proc Natl Acad Sci USA* 95: 3233–3238
- Kuwabara T, Hsieh J, Nakashima K, Taira K, Gage FH (2004) A small modulatory dsRNA specifies the fate of adult neural stem cells. *Cell* 116: 779–793
- Lackinger M, Sungur AO, Daswani R, Soutschek M, Bicker S, Stemmler L, Wust T, Fiore R, Dieterich C, Schwarting RKW et al (2019) A placental mammal-specific microRNA cluster acts as a natural brake for sociability in mice. *EMBO Rep* 20: e46429
- Leung CT, Coulombe PA, Reed RR (2007) Contribution of olfactory neural stem cells to tissue maintenance and regeneration. *Nat Neurosci* 10: 720–726
- Leypold BG, Yu CR, Leinders-Zufall T, Kim MM, Zufall F, Axel R (2002) Altered sexual and social behaviors in *trp2* mutant mice. *Proc Natl Acad Sci USA* 99: 6376–6381
- Li H, Zhong X, Chau KF, Santistevan NJ, Guo W, Kong G, Li X, Kadakia M, Masliah J, Chi J et al (2014) Cell cycle-linked MeCP2 phosphorylation modulates adult neurogenesis involving the Notch signalling pathway. *Nat Commun* 5: 5601
- Liberia T, Martin-Lopez E, Meller SJ, Greer CA (2019) Sequential maturation of olfactory sensory neurons in the mature olfactory epithelium. *eNeuro* 6: ENEURO.0266-19.2019
- Liu Q, Wei W, Coelho CM, Li X, Baker-Andresen D, Dudley K, Ratnu VS, Boskovic Z, Kobor MS, Sun YE et al (2011) The brain-specific microRNA miR-128b regulates the formation of fear-extinction memory. *Nat Neurosci* 14: 1115–1117
- Liu B, Coleman JH, Peterson JN, Zunitch MJ, Jang W, Herrick DB, Schwob JE (2017) Injury induces endogenous reprogramming and dedifferentiation of neuronal progenitors to multipotency. *Cell Stem Cell* 21: 761–774
- Liu G, Yin K, Zhang Q, Gao C, Qiu JL (2019) Modulating chromatin accessibility by transactivation and targeting proximal dsRNAs enhances Cas9 editing efficiency *in vivo*. *Genome Biol* 20: 145
- Liu B, Chen S, Rose A, Chen D, Cao F, Zwinderman M, Kiemel D, Aissi M, Dekker FJ, Haisma HJ (2020) Inhibition of histone deacetylase 1 (HDAC1) and HDAC2 enhances CRISPR/Cas9 genome editing. *Nucleic Acids Res* 48: 517–532
- Livak KJ, Schmittgen TD (2001) Analysis of relative gene expression data using real-time quantitative PCR and the 2(-Delta Delta C(T)) method. *Methods* 25: 402–408
- Long C, Amoasii L, Mireault AA, McAnally JR, Li H, Sanchez-Ortiz E, Bhattacharyya S, Shelton JM, Bassel-Duby R, Olson EN (2016) Postnatal genome editing partially restores dystrophin expression in a mouse model of muscular dystrophy. *Science* 351: 400–403
- Lv X, Jiang H, Liu Y, Lei X, Jiao J (2014) MicroRNA-15b promotes neurogenesis and inhibits neural progenitor proliferation by directly repressing TET3 during early neocortical development. *EMBO Rep* 15: 1305–1314
- Lyons DB, Allen WE, Goh T, Tsai L, Barnea G, Lomvardas S (2013) An epigenetic trap stabilizes singular olfactory receptor expression. *Cell* 154: 325–336
- Mahalik TJ (1996) Apparent apoptotic cell death in the olfactory epithelium of adult rodents: death occurs at different developmental stages. *J Comp Neurol* 372: 457–464
- Majumder S (2006) REST in good times and bad: roles in tumor suppressor and oncogenic activities. *Cell Cycle* 5: 1929–1935
- Mampay M, Sheridan GK (2019) REST: an epigenetic regulator of neuronal stress responses in the young and ageing brain. *Front Neuroendocrinol* 53: 100744
- Mandel G, Fiondella CG, Covey MV, Lu DD, Loturco JJ, Ballas N (2011) Repressor element 1 silencing transcription factor (REST) controls radial migration and temporal neuronal specification during neocortical development. *Proc Natl Acad Sci USA* 108: 16789–16794
- Mellen M, Ayata P, Dewell S, Kriaucionis S, Heintz N (2012) MeCP2 binds to 5hmC enriched within active genes and accessible chromatin in the nervous system. *Cell* 151: 1417–1430

- Mendoza-Viveros L, Chiang CK, Ong JLK, Hegazi S, Cheng AH, Bouchard-Cannon P, Fana M, Lowden C, Zhang P, Bothorel B et al (2017) miR-132/212 modulates seasonal adaptation and dendritic morphology of the central circadian clock. *Cell Rep* 19: 505–520
- Messina A, Langlet F, Chachlaki K, Roa J, Rasika S, Jouy N, Gallet S, Gaytan F, Parkash J, Tena-Sempere M et al (2016) A microRNA switch regulates the rise in hypothalamic GnRH production before puberty. *Nat Neurosci* 19: 835–844
- Mikuni T, Nishiyama J, Sun Y, Kamasawa N, Yasuda R (2016) High-throughput, high-resolution mapping of protein localization in mammalian brain by *in vivo* genome editing. *Cell* 165: 1803–1817
- Miyaoka Y, Berman JR, Cooper SB, Mayerl SJ, Chan AH, Zhang B, Karlin-Neumann GA, Conklin BR (2016) Systematic quantification of HDR and NHEJ reveals effects of locus, nuclease, and cell type on genome-editing. *Sci Rep* 6: 23549
- Monaghan CE, Nechiporuk T, Jeng S, McWeeny SK, Wang J, Rosenfeld MG, Mandel G (2017) REST corepressors RCOR1 and RCOR2 and the repressor INSM1 regulate the proliferation-differentiation balance in the developing brain. *Proc Natl Acad Sci USA* 114: E406–E415
- Montalban-Loro R, Lozano-Urena A, Ito M, Krueger C, Reik W, Ferguson-Smith AC, Ferron SR (2019) TET3 prevents terminal differentiation of adult NSCs by a non-catalytic action at Snrpn. *Nat Commun* 10: 1726
- Nami F, Basiri M, Satarian L, Curtiss C, Baharvand H, Verfaillie C (2018) Strategies for *in vivo* genome editing in nondividing cells. *Trends Biotechnol* 36: 770–786
- Nechiporuk T, McGann J, Mullendorff K, Hsieh J, Wurst W, Floss T, Mandel G (2016) The REST remodeling complex protects genomic integrity during embryonic neurogenesis. *Elife* 5: e09584
- Nishiyama J, Mikuni T, Yasuda R (2017) Virus-mediated genome editing via homology-directed repair in mitotic and postmitotic cells in mammalian brain. *Neuron* 96: 755–768
- Peng C, Li N, Ng YK, Zhang J, Meier F, Theis FJ, Merckenschlager M, Chen W, Wurst W, Prakash N (2012) A unilateral negative feedback loop between miR-200 microRNAs and Sox2/E2F3 controls neural progenitor cell-cycle exit and differentiation. *J Neurosci* 32: 13292–13308
- Perera A, Eisen D, Wagner M, Laube SK, Kunzel AF, Koch S, Steinbacher J, Schulze E, Splith V, Mittermeier N et al (2015) TET3 is recruited by REST for context-specific hydroxymethylation and induction of gene expression. *Cell Rep* 11: 283–294
- Pfeiffer CA, Johnston RE (1994) Hormonal and behavioral responses of male hamsters to females and female odors: roles of olfaction, the vomeronasal system, and sexual experience. *Physiol Behav* 55: 129–138
- Rajman M, Schrott G (2017) MicroRNAs in neural development: from master regulators to fine-tuners. *Development* 144: 2310–2322
- Ran FA, Hsu PD, Wright J, Agarwala V, Scott DA, Zhang F (2013) Genome engineering using the CRISPR-Cas9 system. *Nat Protoc* 8: 2281–2308
- Samulski RJ, Zhu X, Xiao X, Brook JD, Housman DE, Epstein N, Hunter LA (1991) Targeted integration of adeno-associated virus (AAV) into human chromosome 19. *EMBO J* 10: 3941–3950
- Santiago M, Antunes C, Guedes M, Iacovino M, Kyba M, Reik W, Sousa N, Pinto L, Branco MR, Marques CJ (2020) Tet3 regulates cellular identity and DNA methylation in neural progenitor cells. *Cell Mol Life Sci* 77: 2871–2883
- Schwob JE, Youngentob SL, Meiri KF (1994) On the formation of neuromata in the primary olfactory projection. *J Comp Neurol* 340: 361–380
- Selimoglu-Buet D, Rivière J, Ghamlouch H, Bencheikh L, Lacout C, Morabito M, Mb D, Meurice G, Breckler M, Chauveau A et al (2018) A miR-150/TET3 pathway regulates the generation of mouse and human non-classical monocyte subset. *Nat Commun* 9: 5455
- Seth KA, Majzoub JA (2001) Repressor element silencing transcription factor/neuron-restrictive silencing factor (REST/NRSF) can act as an enhancer as well as a repressor of corticotropin-releasing hormone gene transcription. *J Biol Chem* 276: 13917–13923
- Shum EY, Espinoza JL, Ramaiah M, Wilkinson MF (2015) Identification of novel post-transcriptional features in olfactory receptor family mRNAs. *Nucleic Acids Res* 43: 9314–9326
- Sim SE, Lim CS, Kim JI, Seo D, Chun H, Yu NK, Lee J, Kang SJ, Ko HG, Choi JH et al (2016) The brain-enriched microRNA miR-9-3p regulates synaptic plasticity and memory. *J Neurosci* 36: 8641–8652
- Sokpor G, Abbas E, Rosenbusch J, Staiger JF, Tuoc T (2018) Transcriptional and epigenetic control of mammalian olfactory epithelium development. *Mol Neurobiol* 55: 8306–8327
- Soufi A, Dalton S (2016) Cycling through developmental decisions: how cell cycle dynamics control pluripotency, differentiation and reprogramming. *Development* 143: 4301–4311
- Sun YM, Greenway DJ, Johnson R, Street M, Belyaev ND, Deuchars J, Bee T, Wilde S, Buckley NJ (2005) Distinct profiles of REST interactions with its target genes at different stages of neuronal development. *Mol Biol Cell* 16: 5630–5638
- Szulwach KE, Li X, Li Y, Song CX, Wu H, Dai Q, Irier H, Upadhyay AK, Gearing M, Levey AI et al (2011) 5-hmC-mediated epigenetic dynamics during postnatal neurodevelopment and aging. *Nat Neurosci* 14: 1607–1616
- Tan CL, Plotkin JL, Veno MT, von Schimmelmann M, Feinberg P, Mann S, Handler A, Kjemis J, Surmeier DJ, O'Carroll D et al (2013) MicroRNA-128 governs neuronal excitability and motor behavior in mice. *Science* 342: 1254–1258
- Trinh K, Storm DR (2003) Vomeronasal organ detects odorants in absence of signaling through main olfactory epithelium. *Nat Neurosci* 6: 519–525
- Wang G, Achim CL, Hamilton RL, Wiley CA, Soontornniyomkij V (1999) Tyramide signal amplification method in multiplelabel immunofluorescence confocal microscopy. *Methods* 18: 459–464
- Wang Z, Storm DR (2006) Extraction of DNA from mouse tails. *Biotechniques* 41: 410–412
- Wang SZ, Ou J, Zhu LJ, Green MR (2012) Transcription factor ATF5 is required for terminal differentiation and survival of olfactory sensory neurons. *Proc Natl Acad Sci USA* 109: 18589–18594
- Wang G, Guo X, Hong W, Liu Q, Wei T, Lu C, Gao L, Ye D, Zhou Y, Chen J et al (2013) Critical regulation of miR-200/ZEB2 pathway in Oct4/Sox2-induced mesenchymal-to-epithelial transition and induced pluripotent stem cell generation. *Proc Natl Acad Sci USA* 110: 2858–2863
- Williams CL, Uyttingco CR, Green WW, McIntyre JC, Ukhanov K, Zimmerman AD, Shively DT, Zhang L, Nishimura DY, Sheffield VC et al (2017) Gene therapeutic reversal of peripheral olfactory impairment in bardet-biedl syndrome. *Mol Ther* 25: 904–916
- Woldemichael BT, Jawaid A, Kremer EA, Gaur N, Krol J, Marchais A, Mansuy IM (2016) The microRNA cluster miR-183/96/182 contributes to long-term memory in a protein phosphatase 1-dependent manner. *Nat Commun* 7: 12594
- Wong ST, Trinh K, Hacker B, Chan GC, Lowe G, Gaggar A, Xia Z, Gold GH, Storm DR (2000) Disruption of the type III adenylyl cyclase gene leads to peripheral and behavioral anosmia in transgenic mice. *Neuron* 27: 487–497
- Wu J, Xie X (2006) Comparative sequence analysis reveals an intricate network among REST, CREB and miRNA in mediating neuronal gene expression. *Genome Biol* 7: R85

- Wu X, Scott DA, Kriz AJ, Chiu AC, Hsu PD, Dadon DB, Cheng AW, Trevino AE, Konermann S, Chen S *et al* (2014) Genome-wide binding of the CRISPR endonuclease Cas9 in mammalian cells. *Nat Biotechnol* 32: 670–676
- Yang Y, Wang L, Bell P, McMenamin D, He Z, White J, Yu H, Xu C, Morizono H, Musunuru K *et al* (2016) A dual AAV system enables the Cas9-mediated correction of a metabolic liver disease in newborn mice. *Nat Biotechnol* 34: 334–338
- Yarrington RM, Verma S, Schwartz S, Trautman JK, Carroll D (2018) Nucleosomes inhibit target cleavage by CRISPR-Cas9 *in vivo*. *Proc Natl Acad Sci USA* 115: 9351–9358
- Yu W, Mookherjee S, Chaitankar V, Hiriyan S, Kim JW, Brooks M, Ataeijannati Y, Sun X, Dong L, Li T *et al* (2017) Nr1 knockdown by AAV-delivered CRISPR/Cas9 prevents retinal degeneration in mice. *Nat Commun* 8: 14716